Calpains promote α2β1 integrin turnover in nonrecycling integrin pathway

Nina Rintanen[a], Mikko Karjalainen[a], Jonna Alanko[b], Lassi Paavolainen[a], Anita Mäki[a], Liisa Nissinen[c], Moona Lehkonen[a], Katri Kallio[d], R. Holland Cheng[e], Paula Upla[f], Johanna Ivaska[b,g], and Varpu Marjomäki[a]

[a]Department of Biological and Environmental Science/Nanoscience Center, University of Jyväskylä, FI-40351 Jyväskylä, Finland; [b]VTT Technical Research Centre of Finland, FI-20521 Turku, Finland; [c]MediCity Research Laboratory, University of Turku, FI-20014 Turku, Finland; [d]Institute of Biotechnology, University of Helsinki, FI-00014 Helsinki, Finland; [e]Department of Molecular and Cellular Biology, University of California, Davis, Davis, CA 95616; [f]New York Structural Biology Center, New York, NY 10027; [g]Centre for Biotechnology and Department of Biochemistry and Food Chemistry, University of Turku, FI-20520 Turku, Finland

ABSTRACT **Collagen receptor integrins recycle between the plasma membrane and endosomes and facilitate formation and turnover of focal adhesions. In contrast, clustering of α2β1 integrin with antibodies or the human pathogen echovirus 1 (EV1) causes redistribution of α2 integrin to perinuclear multivesicular bodies, α2-MVBs. We show here that the internalized clustered α2 integrin remains in α2-MVBs and is not recycled back to the plasma membrane. Instead, receptor clustering and internalization lead to an accelerated down-regulation of α2β1 integrin compared to the slow turnover of unclustered α2 integrin. EV1 infection or integrin degradation is not associated with proteasomal or autophagosomal processes and shows no significant association with lysosomal pathway. In contrast, degradation is dependent on calpains, such that it is blocked by calpain inhibitors. We show that active calpain is present in α2-MVBs, internalized clustered α2β1 integrin coprecipitates with calpain-1, and calpain enzymes can degrade α2β1 integrin. In conclusion, we identified a novel virus- and clustering-specific pathway that diverts α2β1 integrin from its normal endo/exocytic traffic to a nonrecycling, calpain-dependent degradative endosomal route.**

Monitoring Editor
Robert G. Parton
University of Queensland

Received: Jun 21, 2011
Revised: Nov 23, 2011
Accepted: Nov 30, 2011

INTRODUCTION

Integrins mediate cell attachment to extracellular matrix (ECM) by direct binding to for example, collagen and fibronectin. Binding to ECM causes integrin-dependent formation of focal contacts that are constantly broken and renewed in different locations to facilitate migration and attachment. α2β1 integrin is a collagen-binding integrin associated with important physiological and pathological processes, such as cell migration, inflammation, and cancer. Integrins are constantly endocytosed and recycled back to the plasma membrane. β1 integrin internalization and recycling involve a large number of regulators, including protein kinase Cα (PKCα) and ε (Ng *et al.*, 1999; Ivaska *et al.*, 2005), Arf6 and Rabs 5, 21, and 11, and Rab-coupling protein (Powelka *et al.*, 2004; Pellinen *et al.*, 2006; Caswell *et al.*, 2009).

Binding of another ligand, namely the human echovirus 1 (EV1), to α2β1 integrin does not trigger focal contact formation. The virus–receptor complex is internalized from lipid rafts to the perinuclear cytoplasm, where it accumulates in α2 integrin–enriched multivesicular bodies (α2-MVBs; Marjomäki *et al.*, 2002; Upla *et al.*, 2004; Karjalainen *et al.*, 2008). According to recent data, EV1 prefers binding to the inactive conformation of α2 integrin on the plasma membrane, whereas the active conformation binds to collagen ligand (Jokinen *et al.*, 2010). EV1 binding induces clustering of α2β1 integrin. This can be efficiently mimicked by a sequential treatment with primary anti-α2 and secondary antibodies (Upla *et al.*, 2004). The internalization of the clustered integrins requires Rac1, Pak1, and

This article was published online ahead of print in MBoC in Press (http://www.molbiolcell.org/cgi/doi/10.1091/mbc.E11-06-0548) on December 7, 2011.

Address correspondence to: Varpu Marjomäki (varpu.s.marjomaki@jyu.fi).

Abbreviations used: α2-MVB, α2 integrin–enriched multivesicular bodies; EV1, echovirus 1.

PKCα activation, and the macropinocytic uptake is also facilitated by CtBP/Bars (Karjalainen *et al.*, 2008; Liberali *et al.*, 2008). α2β1 integrin and EV1 remain in the α2-MVBs until the structure releases the virus genome into the cytoplasm, which then promotes the startup of viral replication (Upla *et al.*, 2008).

In addition to EV1, multivesicular endosomes are used by several other viruses, such as human rhinovirus 2 minor group, influenza A, and vesicular stomatitis virus, for their infectious entry into cells (Khor *et al.*, 2003; Le Blanc *et al.*, 2005; Fuchs and Blaas, 2010). The cell surface receptors for viruses are often commonly endocytosed molecules such as integrins or growth factor or chemokine receptors (Mercer *et al.*, 2010). As with their physiological ligands, virus-bound receptors may undergo recycling or down-regulation. According to the classic model for receptor down-regulation, endocytosed receptors are sorted into intraluminal vesicles of multivesicular bodies and further guided to lysosomes for degradation. Degradation occurs in lysosomes by acidic hydrolases, and the degradation may be inhibited by several inhibitors acting on lysosomal hydrolases (Pillay *et al.*, 2002; van der Goot and Gruenberg, 2006). In addition to lysosomes, there are also other cellular machineries that are involved in protein degradation. Polyubiquitinated intracellular proteins can be down-regulated in proteasomes, and entire organelles can be sorted to lysosomes for degradation through macroautophagy or smaller cytosolic components through microautophagy (Ciechanover, 2005).

Calpains are calcium-dependent cytosolic cysteine proteases. Two major isozymes of calpains are calpain-1 and calpain-2, also called μ- and m-calpains, respectively, based on their requirement of calcium for protease activity. In addition to these most common and best-studied forms of calpains, there are also other tissue-specific calpains (Suzuki and Ohno, 1990; Suzuki and Sorimachi, 1998; Goll *et al.*, 2003). More than 100 substrates for calpains have been found, including transcription factors, transmembrane receptors, and cytoskeletal proteins, as well as focal adhesion and signaling molecules (Goll *et al.*, 2003; Franco and Huttenlocher, 2005). In addition, β integrin cytoplasmic domains, including β1 integrin, have been shown to be subjected to calpain cleavage (Pfaff *et al.*, 1999). No specific sequences have been found to act as cleavage sites for calpains, but they instead seem to recognize more-global structural elements (Tompa *et al.*, 2004). Calpain molecule consists of an 80-kDa, large catalytic subunit and a 30-kDa, small regulatory subunit. Autolysis of the 80-kDa catalytic domain to 78- and 76-kDa forms is usually associated with calpain activation, probably by lowering the requirement for calcium (Suzuki and Sorimachi, 1998; Goll *et al.*, 2003; Franco and Huttenlocher, 2005; Hanna *et al.*, 2008). Previously it was shown that in addition to lysosomal degradation, calpain and proteasomal degradation also may contribute to the β1 integrin turnover in cells (Moro *et al.*, 2004).

Here we show that clustering of α2β1 integrin, which mimics EV1 infection, results in efficient internalization and accumulation of the receptor in α2-MVBs. In contrast to the endosomal recycling described for the normal β1 integrin life cycle, clustered α2β1 integrin does not recycle back to the plasma membrane, but instead undergoes down-regulation promoted by calpains in nonlysosomal α2-MVBs.

RESULTS

α2-MVBs are degradative structures

EV1 infection and clustering of α2 integrin with antibodies result in accumulation of the receptor to α2-MVBs (Karjalainen *et al.*, 2008). To investigate integrin traffic along this pathway in more detail, we followed the distribution of unclustered, EV1-bound or antibody-clustered α2 integrin in human osteosarcoma SAOS-α2β1 cells for 6 h. Unclustered α2 integrin (labeled with fluorescent monovalent Fab fragment) was found mainly on the plasma membrane and to some extent in cytosolic vesicles (Figure 1A). In contrast, secondary antibody or EV1 binding induced the clustering of monovalent Fab–α2 integrin conjugate and triggered EV1–α2β1 integrin cointernalization into cytosolic vesicles (Figure 1, B and C, and Supplemental Figure S1A). Of interest, antibody clustering resulted in >60% and EV1 clustering in an even more prominent reduction of the Fab–α2 integrin fluorescence signal between 2 and 6 h. In contrast, no obvious down-regulation of α2β1 signal was observed in the unclustered cells during this time (Figure 1A). The clustering-induced integrin turnover was much accelerated compared with the long half-life of unclustered integrin, as detected with pulse-chase labeling experiments (Figure 1D). To verify that the loss of fluorescence signal was due to degradation of α2 integrin and not only the labeled Fab fragment, two approaches were taken. First, we analyzed integrin down-regulation by comparing signal intensities of endocytosed anti-α2 antibody (MCA2025) with postfixation staining intensities obtained with biotinylated anti–α2 integrin antibody (A211E10) that recognizes another domain of the integrin following internalization for 2 and 24 h. The confocal images showed bright labeling of α2-MVBs after 2 h with both antibodies, but the labeling was considerably reduced after 24 h (Figure 1E). This suggests that the loss in the fluorescence signal was not due to degradation of the endocytosed antibody but indeed integrin down-regulation. Second, we analyzed the turnover rate of α2β1 integrin using surface biotinylation. After surface biotinylation we induced integrin clustering, and after internalization we immunoprecipitated the clustered integrin from lysed cells using the secondary clustering antibody (Figure 1F). The results show that the amount of both α2 and β1 subunits of the clustered heterodimeric integrin decreased significantly during 24 h. In contrast, in the absence of integrin clustering no significant changes were observed in biotinylated receptor levels after 24 h. This result is in line with the metabolic labeling shown in Figure 1D and suggests that, without clustering, the turnover rate of α2β1 integrin is very slow. These results, taken together, demonstrate that α2 integrin is down-regulated after clustering with a much more rapid turnover rate than during normal recycling.

The clustered α2 integrin is not recycled back to the plasma membrane

Because the integrin signal in α2-MVBs decreased with time, we wanted to investigate whether integrin recycling to the plasma membrane was contributing to this. We found that no recycling of the clustered and endocytosed α2 integrin was detected using three independent approaches.

First, we performed a recycling assay based on antibodies that quench Alexa 488 fluorescence on the plasma membrane, as described before (van Kerkhof *et al.*, 2005; Yuseff *et al.*, 2007). After clustering and internalization of α2 integrin with Alexa 488–labeled antibody for 1 h, the plasma membrane fluorescence was quenched with an anti–Alexa 488 antibody (Figure 2A). Quenching was repeated with 1-h intervals during the subsequent 2–5 h of incubation before fixation. Anti–Alexa 488 antibody treatment after 1 h did not markedly reduce the fluorescence, suggesting that the integrin was already efficiently internalized to the cytoplasm. Furthermore, there was no significant difference between the quenched and unquenched samples between 2 and 5 h, indicating that the clustered α2 integrin did not recycle to the plasma membrane. As a comparison, we performed a similar experiment with unclustered α2 integrin. The anti–Alexa 488 treatment after 1 h of internalization showed

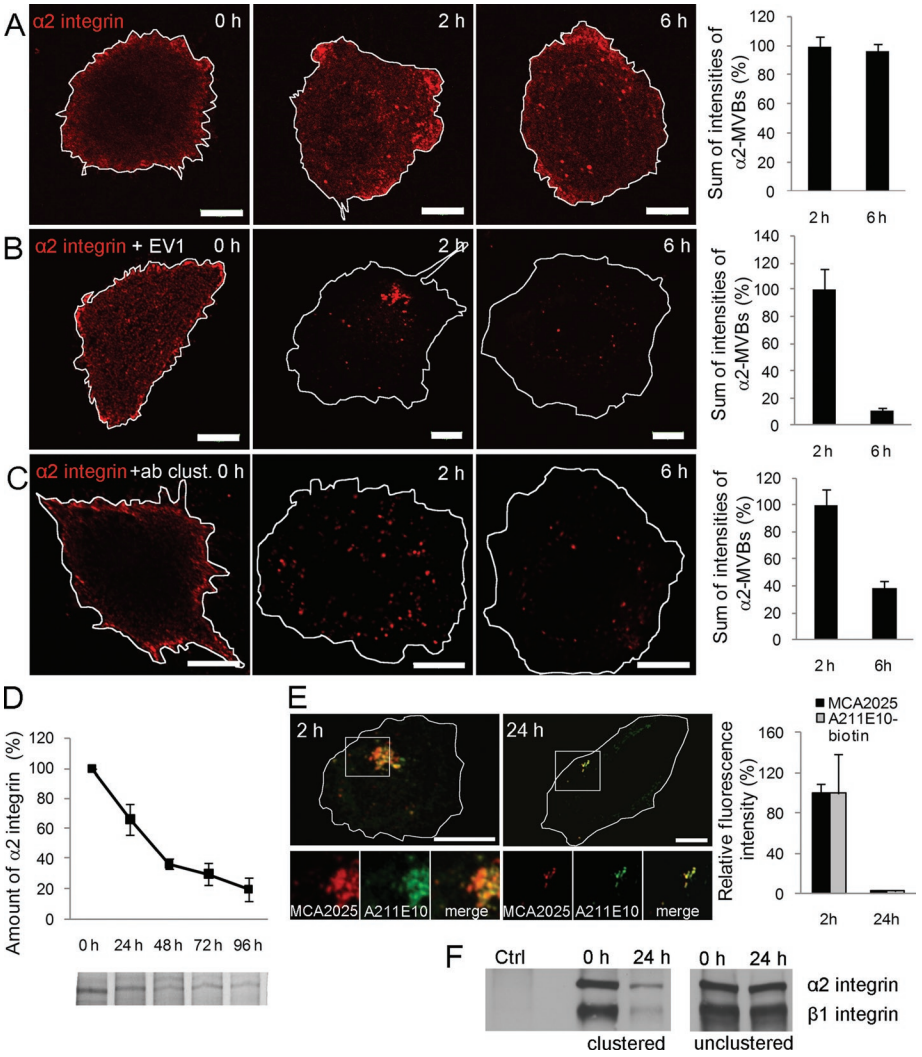

FIGURE 1: Clustered α2 integrin is degraded in α2-MVBs. (A) In SAOS-α2β1 cells, α2 integrin was labeled on the cell surface with anti–α2 integrin antibody (MCA2025) and unclustering goat anti–mouse Fab DyLight 549 fragment. The α2 integrin–Fab conjugate was then internalized for 0, 2, and 6 h and imaged with similar confocal settings. Confocal sections through the cells were projected together. Bars, 10 μm. (B) In addition to α2 integrin–Fab label (described in A), EV1 was bound to cells on ice before internalization. Cells were imaged as described. Bars, 10 μm. (C) α2 integrin was clustered with anti–α2 integrin MCA2025 and clustering goat anti–mouse Alexa 555 antibodies (+ab clust.). Intensity of fluorescence signal (A–C) was measured from confocal three-dimensional sections of single cells. Altogether 30 cells from three independent experiments were analyzed. Mean values ± SE are shown. (D) Normal turnover rate of α2 integrin was determined from metabolically labeled and immunoprecipitated samples. Quantification of gel bands was done with Adobe Photoshop, and the results are shown as averages of three independent experiments (±SE). (E) To evaluate the degradation of α2 integrin in α2-MVBs in more detail, integrin was labeled on the cell surface and after fixation again with another antibody: α2 integrin was first clustered with anti–α2 integrin MCA2025 antibody, followed by clustering with goat anti–mouse Alexa 555 antibody. After internalization for 2 and 24 h, cells were labeled with another antixα2 integrin antibody, biotinylated A211E10, and streptavidin–Alexa 488 (green). Fluorescence intensity was measured from confocal *z*-stacks of 30 cells from three independent experiments (±SE). Bars, 10 μm. (F) Degradation of α2 integrin was followed also after surface biotinylation of all proteins and by immunoprecipitating the integrin clusters (clustered) or unclustered α2 integrin (unclustered) via the clustering antibody or integrin antibody, respectively. Control cells were treated with the clustering secondary antibody without the primary antibody.

that 70% of the α2 integrin pool was sensitive to the treatment, suggesting that the majority of α2 integrin was on the plasma membrane (Figure 2B). Comparison of the fluorescence intensities with or without the subsequent anti–Alexa 488 treatments showed somewhat higher values for the unquenched control intensities, suggesting a slow recycling of the control integrin back to the plasma membrane.

Second, we performed a fluorescence photobleaching experiment in order to see whether the clustered and internalized fluorescent integrin was recycling back to the plasma membrane. Before bleaching and internalization, the clustered α2 integrin labeling showed a typical diffuse appearance of small clusters throughout the cell surface (Figure 2C, Ctrl). After a 2.5-h internalization period virus-clustered integrin showed large vesicle accumulations in the cytoplasm beside the nucleus. Fluorescence was bleached from the cell outside of the perinuclear vesicles, and the appearance of fluorescence to cell edges was monitored using 1-h intervals. These data show that the perinuclear α2-MVBs remained mainly static and that the cytoplasmic and plasma membrane fluorescence signal did not increase after bleaching, suggesting that recycling did not occur during the total follow-up period of 6.5 h (Figure 2C).

Third, we labeled the α2 integrins for electron microscopy using antibody-conjugated protein A–gold (PA-gold) as described before (Upla *et al.*, 2004) and measured the areas of the α2 integrin–positive structures and their distances from the nucleus (Figure 2D and Supplemental Figure S1B). In addition, we determined the number of PA-gold patches on the cell membrane. We found that the distance of α2 integrin structures from the nucleus did not change between the 2- and 24-h time points, suggesting that structures were located in the same perinuclear area in the cell at both time points. In addition, the quantified area of the vesicles remained similar after 2 and 24 h. Furthermore, the number of PA-gold positive patches on the plasma membrane did not increase after 2 h, further suggesting that there was no recycling of integrin between 2 and 24 h.

Taken together, the data from these three independent approaches unambiguously demonstrate that integrin is not recycled after clustering and further suggest that the intensity reduction observed in the α2-MVBs may be due to integrin degradation in the vesicles.

α2-MVBs do not overlap with lysosomal markers

The down-regulation of numerous ligands and receptors targeted to multivesicular bodies is suggested to take place in lysosomes by acid hydrolases in low pH. Of interest, recent data indicate that α5 integrin can be guided to lysosomal degradation together with fibronectin in migrating fibroblasts (Lobert *et al.*,

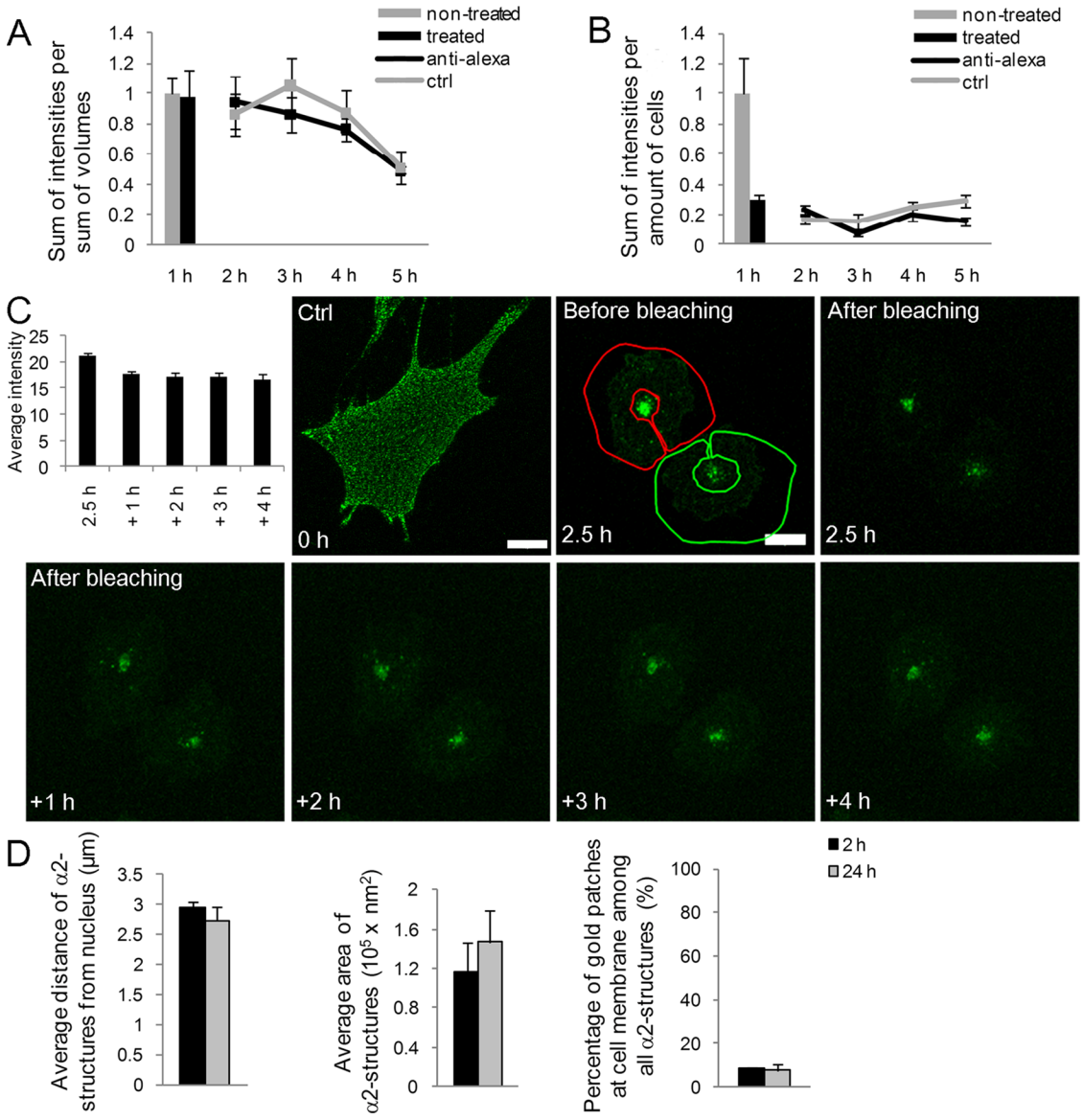

FIGURE 2: Clustered α2 integrin is not recycled back to the plasma membrane. Recycling of (A) clustered and (B) unclustered α2 integrin was analyzed in SAOS-α2β1 cells by measuring the fluorescence intensity of surface-labeled integrin (Alexa 488) using repetitive treatments with the quenching anti–Alexa 488 antibodies. First, integrin was allowed to internalize for 1 h at 37°C and then treated with anti–Alexa 488 on ice for 30 min. Anti–Alexa 488 antibody treatment was thereafter repeated after 1-h intervals during subsequent incubations at 37°C for 4 h. Fluorescence intensity was measured from confocal *z*-stacks of images containing several cells. Altogether more than 50 cells from three independent experiments were analyzed. Results are shown as normalized mean values (±SE). (C) Recycling of α2 integrin from α2-MVBs back to plasma membrane was followed in living cells. Fab-DyLight 488–labeled α2 integrin was clustered with EV1 and internalized for 2.5 h. The edges of the cells were bleached, and trafficking of α2 integrin was observed at 1-h intervals. Average intensity of the bleached areas was quantified from three-dimensional sections. Bars, 10 μm. (D) The localization and size of α2 integrin–positive structures were determined from electron microscopy samples. First, anti–α2 integrin antibody was bound on cells on ice, followed by the clustering secondary antibody (rabbit anti-mouse) and protein A gold (10 nm). The gold clusters were allowed to internalize for 2 and 24 h. The size and location of gold particle positive structures were measured from 15 cells from two separate experiments (±SE) with iTEM software (Olympus). Altogether 75 and 108 vesicles were measured at 2 or 24 h, respectively.

2010). Because our recent data suggested that α2-MVBs are not particularly acidic and lack many tested markers of the clathrin-dependent pathway (Karjalainen *et al.*, 2011), we wanted to characterize these novel MVBs more carefully both by electron microscopy (EM) and confocal microscopy.

EM of internalized clustered α2β1 integrin showed rather large tubulovesicular structures during early time points, for example, 15 min postinfection (p.i.; Figure 3), and only 23% of the structures show intraluminal vesicles (ILVs), the hallmark of MVBs (Karjalainen *et al.* 2008). However, already at 30 min p.i., the number of larger vesicular structures with ILVs clearly increased (~45%). After 2 and 3 h, already 72 and 90% of the structures are matured multivesicular bodies, respectively. EM observations after 6 h verify that the structures no longer show any signs of tubulovesicular "early elemental"

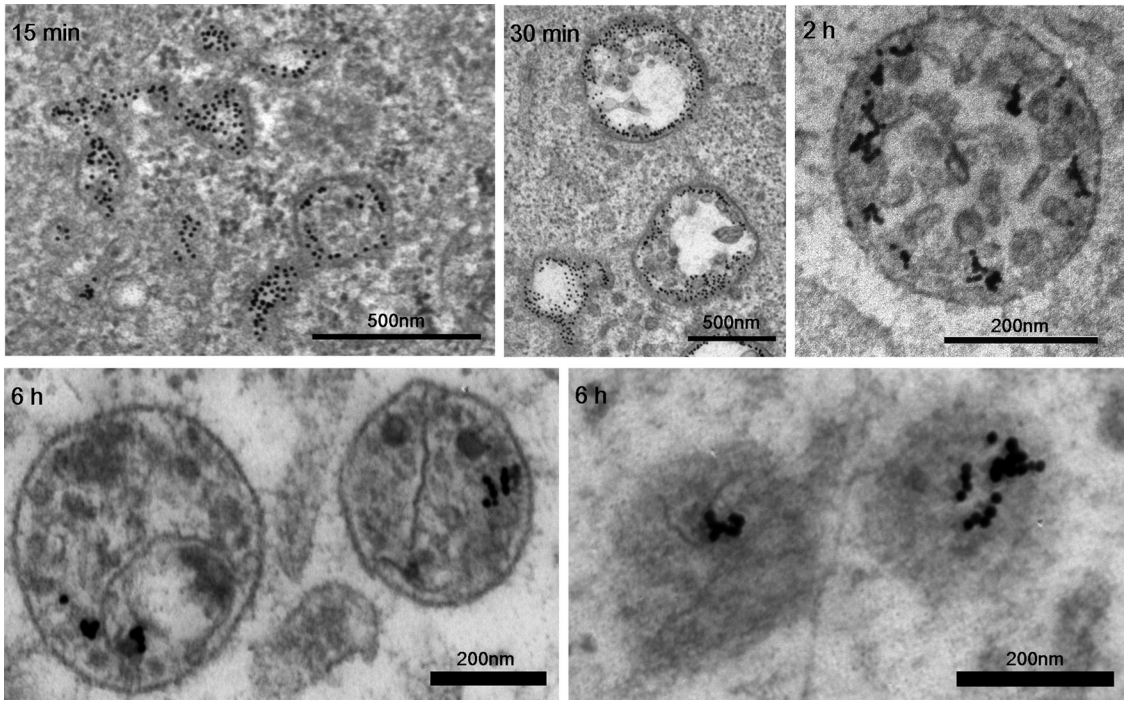

FIGURE 3: EM images of endosomes triggered after α2β1 integrin clustering. Internalization for shorter time periods—for example, 15 min—shows structures that have tubular extensions and vesicular parts without clear ILVs. ILVs grow continuously during internalization, and after 30 min >45% of the structures show several ILVs. The majority of the structures after 2 h and later are MVBs with a high number of ILVs. After 6 h, the number of clearly defined ILVs seemed to have decreased, and for some structures the limiting membrane is also less conspicuous (lower right). Integrin was labeled on the plasma membrane with specific primary antibodies, followed by secondary antibodies and protein A gold (10 nm). Bars, 200 and 500 nm.

characteristics. Furthermore, after 6 h, structures occasionally with less clearly defined ILVs or inner material and less conspicuous limiting membrane were observed, suggesting that some sort of degradation may occur inside α2-MVBs.

The early time points showing tubulovesicular structures were also characterized by confocal labeling for early endosomal marker (EEA1; Figure 4A and Supplemental Figure S1C). EV1 did not colocalize with EEA1 after 5 or 15 min. The 30-min (Figure 4A) and 1- and 2-h (Supplemental Figure S1C) time points were also labeled with late endosomal/lysosomal markers CD63, Lamp-1, and Rab7. None of these markers showed any colocalization with EV1 or α2β1 integrin.

A more careful, quantitative measurement of the colocalization was performed for the time points between 2 and 6 h with Lamp-1 and CD63. These measurements showed only random background colocalization (<10%) with internalized EV1 (Figure 4B). Similarly, cation-independent mannose-6-phosphate receptor (CI-MPR), which is located mainly in the *trans*-Golgi network and late endosomes, showed negligible colocalization (<10%) with α2 integrin antibody at 1, 2, or 6 h after clustering (Supplemental Figure S1D). Furthermore, Rab7 showed no significant colocalization with internalized α2 integrin between 1 and 6 h of clustering (Figure 4B), and no colocalization was found with 1,1′-dioctadecyl-3,3,3′,3′-tetramethylindocarbocyanine–low-density lipoprotein (Dil-LDL) internalized to lysosomes (Supplemental Figure S1E). On the basis of these data, we conclude that the α2-MVBs created by EV1 or antibody clustering are distinct from the endosomes along the clathrin-dependent pathway and do not interact with lysosomes.

α2-MVBs are not highly acidic

Because low endosomal pH is known to be critical for cargo degradation, at least in lysosomes, we were interested in measuring the intraendosomal pH in α2-MVBs at late time points. In line with the negligible labeling with lysotracker in our previous studies (Pietiäinen *et al.* 2004; Karjalainen *et al.*, 2011), these endosomes showed close-to-neutral pH values during the first 3 h of internalization (Karjalainen *et al.*, 2011). We used a similar protocol here for later time points relevant for degradation and included two different antibody conjugates in the integrin clustering protocol—a pH-stable Alexa 555 conjugate and a pH-sensitive fluorescein isothiocyanate (FITC) conjugate. The fluorescence intensity ratio between FITC and Alexa 555 was measured from internalized vesicles at different time points and compared with a pH-standard curve that was prepared in the same live assay. The pH of EV1-induced α2-MVBs after 6 h decreased to a slightly acidic pH of 6.8 (Figure 5A). Without EV1, the pH of endosomes after antibody-induced clustering was 6.9 and 6.5 after 3 and 8 h, respectively. As a control for normal vesicle acidification in the lysosomal pathway, we performed a similar experiment for epidermal growth factor receptor (EGFR), which is targeted to lysosomes for degradation upon stimulation with 100 ng/ml EGF. For the assay we used an antibody against the luminal domain of EGFR that does not interfere with EGF binding. EGF stimulation for 1, 2, and 4 h showed EGFR in more acidic structures, with pH between 5.2 and 5.5 (Figure 5A). Bafilomycin treatment of EGFR-containing endosomes or EV1-induced α2-MVBs increased the pH to neutral values as expected.

Because bafilomycin treatment had some effect on the intraendosomal pH, we also tested its effect on both infectivity and cargo

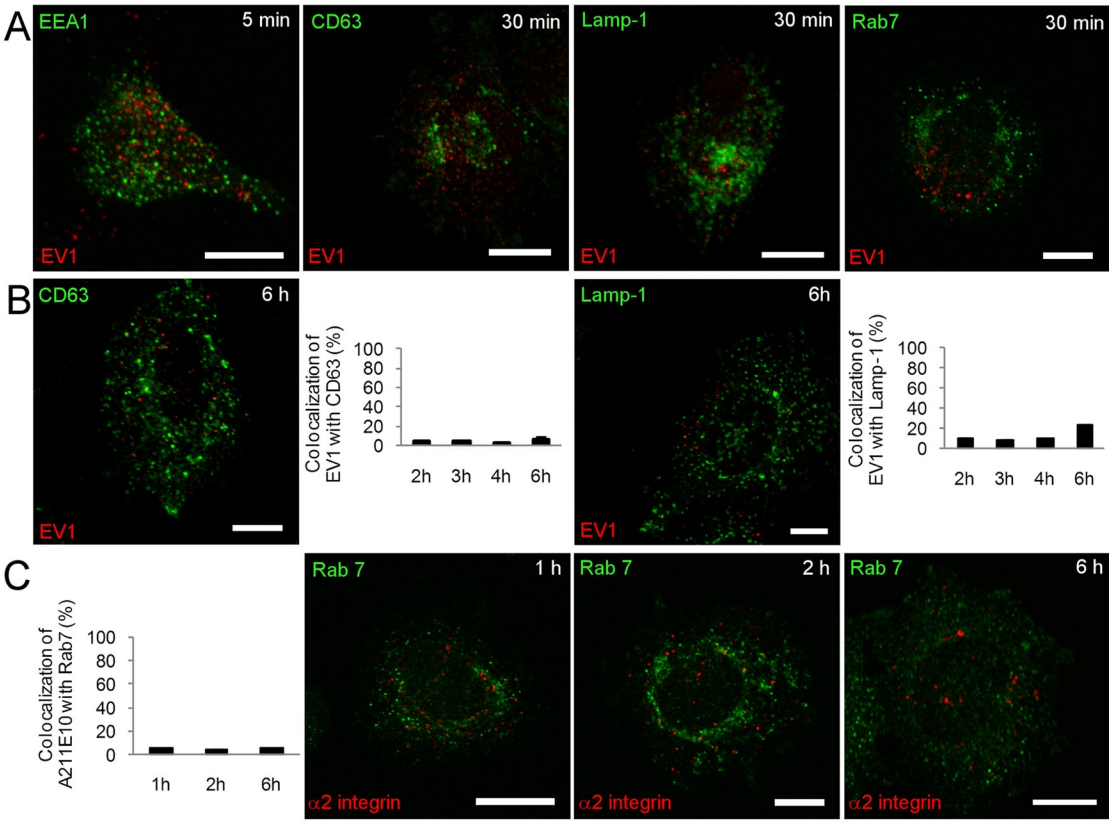

FIGURE 4: The integrin internalization pathway has no significant association with the acidic clathrin-dependent pathway. (A) Colocalization of the early endosomal marker EEA1 (green) with EV1 after 5 min and of the classic late endosomal/lysosomal markers CD63 and Lamp-1 (green) with EV1 (red) and Rab7 (green) with α2 integrin (red) after 30 min of internalization. Quantifications of colocalization of (B) EV1 with Lamp-1 and CD63 and (C) Rab7 (green) with α2 integrin for later time points were done from confocal single sections of single cells using a colocalization tool in the BioImageXD software. Altogether 30 cells from three independent experiments were analyzed. Results are shown as mean values ± SE. Bars, 10 μm.

degradation. We added bafilomycin at different time points p.i. and allowed the infection to proceed until 6 h. We found that bafilomycin had an effect on EV1 infection if administered during early phase of infection. When bafilomycin was added 2 h p.i., the effect was no longer significant, suggesting that the early entry phase, possibly virus uncoating, was sensitive for the bafilomycin effect (Figure 5B). However, later, when the α2-MVBs are known to be fully matured as judged by electron microscopy and the structures are about to open for genome release to the cytoplasm, pH no longer played a role in EV1 infection.

We also measured the effect of bafilomycin on α2 integrin degradation after clustering with antibodies between 2 and 6 h. The results showed that bafilomycin had a small inhibitory effect on the degradation (Figure 5C). The results, taken together, thus suggest that the EV1-induced α2-MVBs do not require extensive acidification of the structures for late stages of infection and for down-regulation of α2 integrin.

Connection to proteasomal or autophagosomal degradation

Because there was no significant connection of α2 integrin degradation or EV1 infection to the lysosomal pathway and degradation, we tested the effect of two well-characterized proteasomal inhibitors, lactacystin and bortezomib, on α2 integrin–associated cargo degradation. Measurements of integrin-conjugated horseradish peroxidase (HRP) signal after 6 h of internalization showed that these inhibitors did not have any effect on the degradation of α2-conjugated HRP (Figure 6A). Furthermore, neither drug could block EV1 infection, further suggesting that proteasomal activity was not involved in α2-MVB function (Figure 6B).

Another form of degradation is autophagy. It depends on calpains, since in calpain-deficient cells autophagy is impaired and lysosomal activity is reduced (Demarchi *et al.*, 2006). The EV1-related viruses coxsackieviruses B3 and B4 have been shown to use autophagosomes in their replication (Wong *et al.*, 2008; Yoon *et al.*, 2008), and both viruses need calpains for their infection (Upla *et al.*, 2008; Yoon *et al.*, 2008). Thus we checked the connection of EV1 and α2 integrin to autophagosomes by overexpressing the autophagosomal marker LC3–green fluorescent protein (GFP). Infectivity measurements showed that LC3-GFP overexpression did not promote, but rather inhibited, EV1 infection compared with GFP-transfected control cells (Figure 6C). We also determined the amount of LC3-GFP–positive structures of EV1-infected and control cells and found that EV1 infection did not increase the amount or size of LC3-GFP structures (Figure 6D), in contrast to coxsackievirus B3, which increased the number and size of these structures (Wong *et al.*, 2008). In addition, we did not detect any significant colocalization between LC3 and α2 integrin, suggesting that α2-MVBs are not associated with the autophagosomal system (Figure 6E). Although these data do not conclusively rule out autophagocytosis, they suggest that EV1 does not need autophagosomes in its

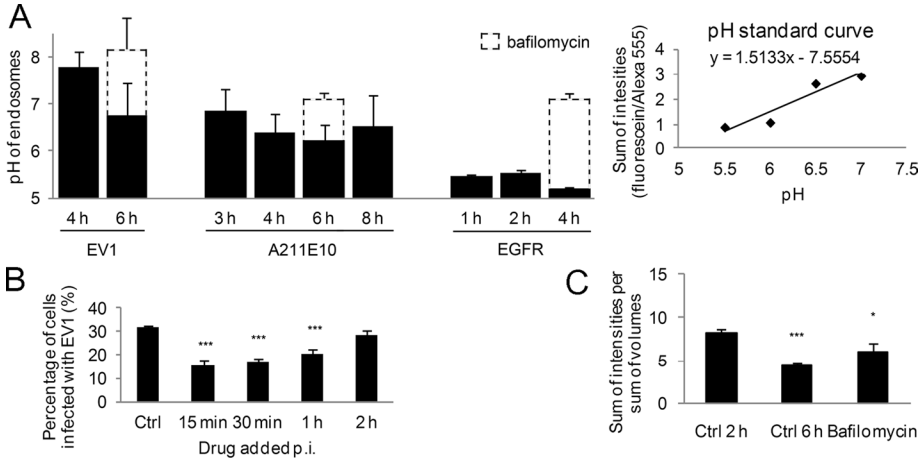

FIGURE 5: Significant acidification is not required for α2 integrin degradation and EV1 infection. (A) pH of α2-MVBs after α2 integrin clustering with EV1, A211E10, and EGFR ± bafilomycin was measured from live SAOS-α2β1 cell images as described in *Materials and Methods*. The ratio between goat anti–rabbit/mouse FITC and goat anti–rabbit/mouse Alexa 555 signal, bound at 1:1 stoichiometric ratio to anti-EV1 antibody on the plasma membrane before internalization, was measured from each time point and compared with the pH standard curve. The pH standard curve was acquired by measuring ratios of virus-bound dyes in the presence of different pH buffer solutions supplemented with nigericin (20 μM). The results were analyzed from 15 to 30 confocal sections, and the experiments were repeated two (EV1) to four (α2 integrin) times (±SE). (B) Effect of 50 nM bafilomycin on EV1 infection rate was determined. The drug was added 15 min, 30 min, 1 h, or 2 h p.i. Infection was calculated from >750 cells from three individual experiments (±SE). Statistical significance was tested with Student's *t* test (***$p < 0.001$). (C) The effect of bafilomycin (50 nM) on α2 integrin fluorescence intensities was measured between 2 and 6 h of internalization. Quantification was done from confocal sections of 30 microscope images containing at least 20 cells each from three independent experiments (±SE). Statistical significance was tested with Student's *t* test (*$p < 0.05$, ***$p < 0.001$).

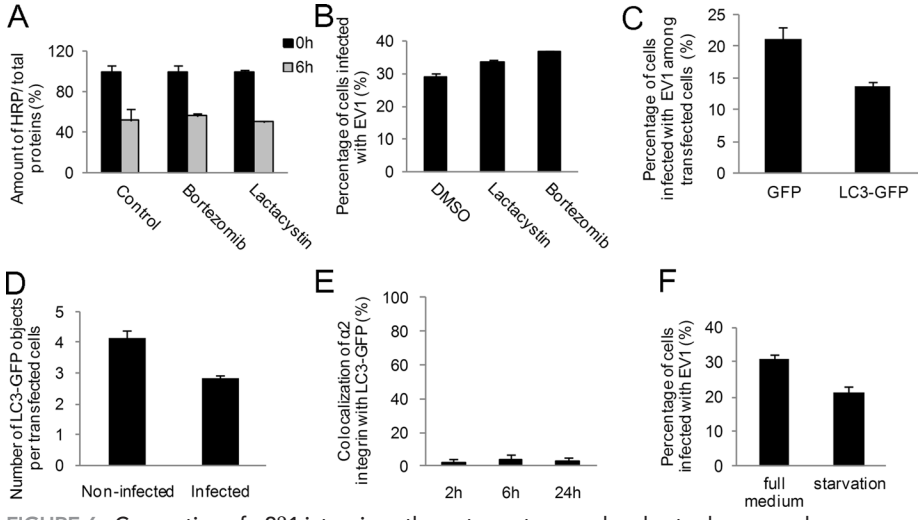

FIGURE 6: Connection of α2β1 integrin pathway to proteasomal and autophagosomal degradation. Effect of proteasome inhibitors lactacystin (10 μM) and bortezomib (0.7 μM), on (A) the activity of α2 integrin–conjugated HRP and (B) EV1 infection. For EV1 infectivity, calculations of >750 cells from three independent experiments were analyzed. Results are shown as mean values (±SE). C) Infection rate in SAOS-α2β1 cells transfected with GFP (control) or LC3-GFP was counted from at least 750 cells and three independent experiments. Results are shown as averages (±SE). (D) The amount of LC3-GFP structures per cell at 3 h p.i. was calculated in noninfected (control) and infected cells. Altogether 200 cells were calculated from three independent experiments, and results are shown as mean values (±SE). (E) Quantification of colocalization between clustered and internalized α2 integrin and the transfected autophagosomal marker LC3-GFP was performed. Quantification was done from single confocal sections with the colocalization tool in the BioImageXD software. Calculations were done from 30 cells from three independent experiments (±SE). (F) Infectivity of EV1 was tested after overnight serum-free starvation or during full medium conditions. A minimum of 750 cells was counted from three independent tests. Results are presented as average of three experiments (±SE).

infection process and that EV1 infection itself does not cause appearance of enlarged LC3-GFP structures (Supplemental Figure S2A). Finally, infectivity measurements after extended serum-free starvation of cells showed lowered infectivity compared with higher serum concentrations (Figure 6F). Given that serum starvation is known to drive autophagocytosis, this result is also in line with the suggestion that autophagocytosis may not be crucial for EV1 infection and that autophagocytosis is not associated with this integrin internalization pathway.

Degradation of integrin cargo depends on calpains

We showed previously that the neutral proteases calpains are essential for EV1 infection and that they are associated with internalized EV1 and α2β1 integrin (Upla *et al.*, 2008). Therefore we decided to test whether they were also contributing to the degradation of clustered α2 integrin. We first tested the involvement of calpains during the antibody-induced clustering with Alexa conjugate in confocal microscopy (Figure 7A). In normal clustering (=control), integrin signal accumulated during 2 h in perinuclear vesicles, and the signal gradually diminished, so that after 24 h almost all signal was gone. This was partially reversed by the pan inhibitor of calpains calpeptin. Leupeptin, which inhibits lysosomal degradation, showed only a modest inhibition of α2 degradation.

In addition to fluorescence intensity measurements, we performed an analogous experiment using HRP conjugate in clustering. These data also show that in control cells the HRP signal decreased by roughly 60% after 6 h, and it was practically undetectable after 24 h (Figure 7B). However, calpeptin, but not leupeptin, efficiently inhibited the degradation of the HRP cargo. In addition to calpeptin, specific calpain 1 and 2 inhibitors also inhibited α2 integrin downregulation (Supplemental Figure S2B). This further suggests a role of both calpain-1 and calpain-2 in the degradation process. The inhibitory effect was specific to calpain inhibitors since other protease inhibitors had no effect on degradation (Supplemental Figure S2C). Because calpains seemed to promote the degradation of the HRP signal, we then wanted to verify whether α2β1 integrin could also be degraded by calpain proteases in vitro. We incubated α2 integrin, immunoprecipitated from metabolically labeled cells, with calpain-1 or calpain-2 for 5 and 60 min (Figure 7C). The results showed that both types of calpains were able to degrade α2 integrin in vitro, with increasing degradation following 60 min of incubation.

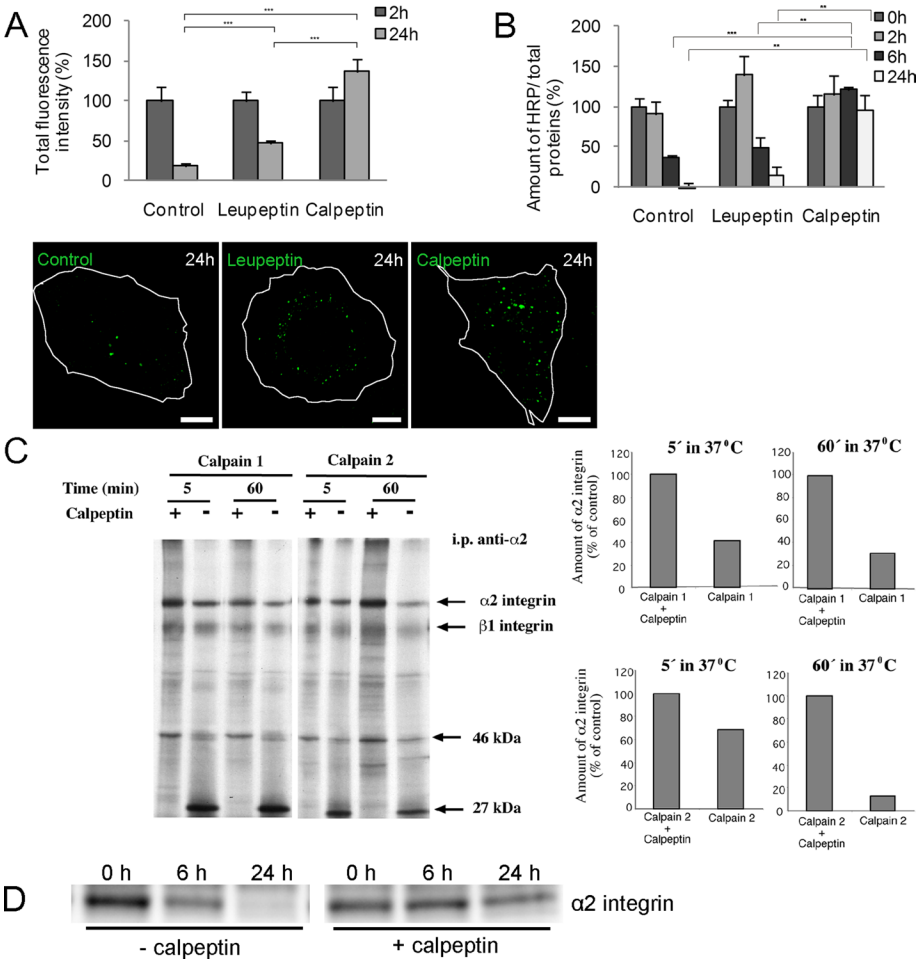

FIGURE 7: Calpain inhibitor blocks degradation of α2 integrin. (A) Influence of leupeptin and calpeptin on the fluorescence intensity of integrin-conjugated Alexa 488 after α2 integrin clustering and internalization in SAOS-α2β1 cells. Fluorescence signal was quantified from single confocal sections. Altogether 30 cells from three independent experiments were calculated (±SE) Statistical significance was tested with Student's *t* test (***$p < 0.001$). Bars, 10 μm. (B) Effect of leupeptin and calpeptin on the amount of HRP activity, conjugated to clustering secondary antibody, was measured. The amount of HRP was measured from cell lysates. Cells were pretreated overnight with DMSO (control) and leupeptin (50 μg/ml) or for 1 h with calpeptin (50 μM). Results are averages of three independent experiments (±SE). Statistical tests were done with Student's *t* test (**$p < 0.01$, ***$p < 0.001$). (C) Metabolically labeled and immunoprecipitated α2 integrin samples were treated with calpain-1 or calpain-2 for 5 and 60 min at 37°C. In control samples, the calpain inhibitor calpeptin was added before calpain enzymes. Densitometric quantitation of α2 integrin levels was done with ImageJ. (D) Immunoprecipitation of surface-labeled α2 integrin via the clustering antibody introduced before internalization for 0, 6, and 24 h with or without the presence of calpeptin. α2 integrin was revealed on the blot by immunolabeling.

The degradation was seen as the disappearance of the ~160-kDa α2 integrin band and the ~130-kDa β1 integrin band. Simultaneously, a small band of ~27 kDa accumulated with calpain induced degradation but was absent in calpeptin-treated lysates. This calpain-induced degradation of α2 integrin was inhibited when the specific calpain inhibitor calpeptin was present.

The inhibitory effect of calpeptin on integrin degradation was also tested after immunoprecipitation of integrins clustered and internalized from the plasma membrane (Figure 7D). Immunoprecipitation of the clusters via the clustering antibody showed typically lower amount of α2 integrin after 6 h and very little after 24 h. Immunoprecipitation of the clusters in the presence of calpeptin showed more α2 integrin precipitated after 6 and 24 h, suggesting that calpeptin could inhibit integrin degradation. The ability of calpain inhibitors to block α2 integrin degradation was not due to inhibition of the formation of α2-MVB structures. This was evident because administration of the calpain inhibitors at 2 h postinternalization was still sufficient to inhibit integrin degradation (Supplemental Figure S2D).

Calpains are active and present in α2-MVBs

Because calpains are known to be localized in the cytosol and bound to their substrates also on the membranes, we wanted to study in greater detail how these cytosolic neutral proteases are associated with α2-MVBs. We first performed immunoprecipitation of α2β1 integrin using different approaches. Immunoprecipitation of α2 integrin with α2 integrin polyclonal antibody (pAb) from both unclustered and clustered cells after 2 h of internalization showed a significant fraction of calpain-1 in the immunoisolates (Figure 8). The amount of calpain-1 associated with α2 integrin isolated from the total integrin pool did not change due to clustering, suggesting that clustering itself caused no major change in the amount of calpain-1 associated with total α2 integrin. Similar data were obtained with two different β1 integrin antibodies in conjunction with EV1 infection. Of interest, EV1-induced clustering promoted coprecipitation predominantly with the smaller, possibly activated form of calpain-1, whereas in the lysate, the 80-kDa form of calpain was most abundant. Finally, as the third approach, immunoprecipitation was performed using the clustering rabbit anti-mouse antibody that was bound on the integrin antibodies on the plasma membrane before internalization. Immunoprecipitation of this clustering antibody thus precipitated only the integrin clusters that were internalized to the cytoplasm during 15 min and 2 h. The results show that calpain-1 was also enriched with integrin clusters after 2 h of clustering, proving that calpain was present in the internalized α2-MVBs. Taken together these results show that both the clustered and unclustered α2β1 integrin associates with calpain-1 and further suggest that, after clustering, a higher amount of coprecipitated calpain-1 is associated with α2β1 integrin clusters at a later time point.

In line with the observed association of calpains with internalized α2β1 integrin, we detected low but significant labeling of calpain-2 in α2-MVBs after 2 and 6 h in thin, frozen sections (Figure 9A). Careful quantitation of small gold particles representing calpain label in α2-MVBs against labeling with control immunoglobulin G (IgG) showed that α2-MVBs after both 2 h ($p < 0.005$) and 6 h ($p < 0.0002$) were significantly labeled with calpain-2. The labeling showed that calpain was present inside the α2-MVBs.

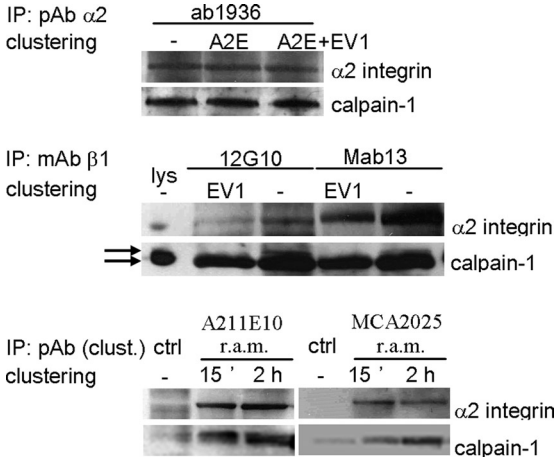

FIGURE 8: Calpains are present in α2-MVBs. Immunoblot labeling of calpain-1 and α2 integrin from SAOS-α2β1 cell lysates (lys) or after immunoprecipitation was performed. Immunoprecipitation of total α2 or β1 integrin pool from cell lysates with or without α2 integrin clustering was performed with polyclonal α2 integrin (pAb, ab1936) or monoclonal β1 integrin (mAb, 12G10, and Mab13) antibodies. A pool of clustered α2β1 integrins was specifically precipitated with the rabbit anti-mouse (r.a.m.) antibody that was used for clustering of the α2 integrin mAbs (MCA2025, A211E10, A2E). The 80-kDa and a smaller form of calpain-1 are indicated by arrows.

Furthermore, the α2-MVB–associated calpain was active. The total calpain activity (detected with cell-permeable fluorogenic calpain substrate 7-amino-4-chloromethylcoumarin, t-BOC-L-leucyl-L-methionine amide [t-BOC]; Rosser *et al.*, 1993) after α2 integrin clustering for 30 min and 2 h was close to the basal control activity in the cells (Figure 9B), in line with our earlier calpain measurements using a different approach (Upla *et al.*, 2008). However, already after 30 min and also later, at 2 h, the calpain activity was detected in the α2-MVBs in the cytoplasm, suggesting that redistribution of cytoplasmic calpain occurred to α2 integrin–positive structures (Supplemental Figure S3A). Colocalization measurements showed that ~80% of the t-BOC label colocalized with α2 integrin at 2 h p.i., suggesting that after integrin clustering, the majority of the highest calpain activity was localized to α2-MVBs (Figure 9C). Six hours of integrin clustering with or without EV1 caused an increase of calpain activity (Figure 9B). According to the microscopy, this was due to the higher activity in α2-MVBs, but also in the cytoplasm, elevating the overall cellular activity above the basal activity. Treatment of the cells with calpeptin abolished calpain activation and, as expected, showed very little intensity when imaged with similar settings (Supplemental Figure S3A). In conclusion, these results demonstrate that active calpain is present in the α2-MVBs after integrin clustering and internalization. Thus, clustering of α2 integrin induces its internalization into a nonrecycling, nonlysosomal endosomal compartment where the receptor is degraded by calpains.

Collagen uptake induces α2β1 integrin internalization and promotes calpain-sensitive turnover of integrin

Because it is very probable that viruses induce pathways that were originally developed for physiological ligands, we decided to study whether collagen type I has similar effects on α2β1 integrin distribution. Indeed, plating the cells on collagen type I caused redistribution of integrin to the cytoplasm (Figure 10). The number and size of the internalized vesicles seemed to increase from 2 to 6 h. Double labeling with collagen showed that internalized α2β1 integrin colocalized at least partially with collagen. The colocalization was more obvious when more integrin also was internalized, that is, after 6 h. However, it is striking that, after 24 h, the cytoplasmic integrin vesicles disappeared and the overall amount of α2β1 integrin seemed to have dropped to levels lower than that in cells grown on plastic. This suggested that the integrin might have undergone degradation. In addition to steady-state labeling of α2β1 integrin, we also followed α2β1 integrin labeled on the cell surface with monovalent Fab fragment and fluorescent conjugate 2 h after plating on collagen. At 2 h after labeling (4 h in total after plating on collagen) the label was only detected in cytoplasmic vesicles, in contrast to control Fab labeling on plastic, which showed more plasma membrane labeling (Figure 10C). Treatment of the cells with calpeptin caused the accumulation of integrin with collagen into cytoplasmic vesicles with no apparent loss of integrin signal in cytoplasmic vesicles after 24 h (Figure 10A). Of interest, colabeling of the collagen and Lamp-1, the late endosomal/lysosomal marker, showed no colocalization after 6 or 24 h, suggesting that, similar to internalized α2β1 integrin, collagen also did not enter acidic lysosomal structures during the first 24 h (Supplemental Figure S3B). Treatment of the cells with calpeptin did not cause any change in the colocalization of collagen with Lamp-1.

These results suggest that collagen uptake induces a comparable internalization and enhanced turnover of α2β1 integrin to integrin clustering with EV1. Furthermore, internalized α2β1 integrin colocalizes at least partially with endosomal collagen, and this colocalization is enhanced when integrin turnover is blocked with calpain inhibition.

DISCUSSION

Integrins mediate cell attachment to its environment by binding to ECM components, such as collagen, fibronectin, vitronectin, and laminin (van der Flier and Sonnenberg, 2001). Especially in migrating and proliferating cells, disintegration and formation of adhesion sites are crucial. For continuous turnover of focal adhesions, integrins are recycled through the recycling pathways involving early and recycling endosomes that are regulated by rab4/5 and rab11/Arf6/Arf1/Rab5/Rab25/Rab21, respectively (for reviews see Jones *et al.*, 2006; Pellinen and Ivaska, 2006). In addition, ligand-bound integrins may be targeted to the lysosomes for degradation (Lobert *et al.*, 2010). In this study we show that α2β1 integrin clustering by EV1 or by antibodies triggers endocytosis of virus and the receptor to specialized perinuclear α2 integrin–rich multivesicular bodies, α2-MVBs. This EV1-triggered integrin traffic route is markedly distinct from the previously described integrin traffic routes for several reasons: 1) the endocytosed integrin is not recycled back to the plasma membrane; 2) the integrin is not targeted to lysosomes for degradation; and 3) the integrin degradation occurs in less acidic α2-MVBs, which are biochemically distinct from conventional MVBs.

Proteins of the plasma membrane are normally down-regulated in lysosomes by acidic hydrolases. Those include growth factor receptors, such as EGFR or vascular endothelial growth factor receptor 2, which are guided to acidic late endosomes/lysosomes after stimulation (Futter *et al.*, 1996; Falguieres *et al.*, 2009; Bruns *et al.*, 2010). EGF stimulation causes rapid proteolysis of EGFR, which is almost complete in 2 h (Burke *et al.*, 2001; Salazar and Gonzalez, 2002; Sigismund *et al.*, 2008). In contrast, α2 integrin down-regulation after clustering was a much slower process than classic lysosomal degradation. This is in line with our data showing that lysosomal degradation is not involved in α2 integrin down-regulation.

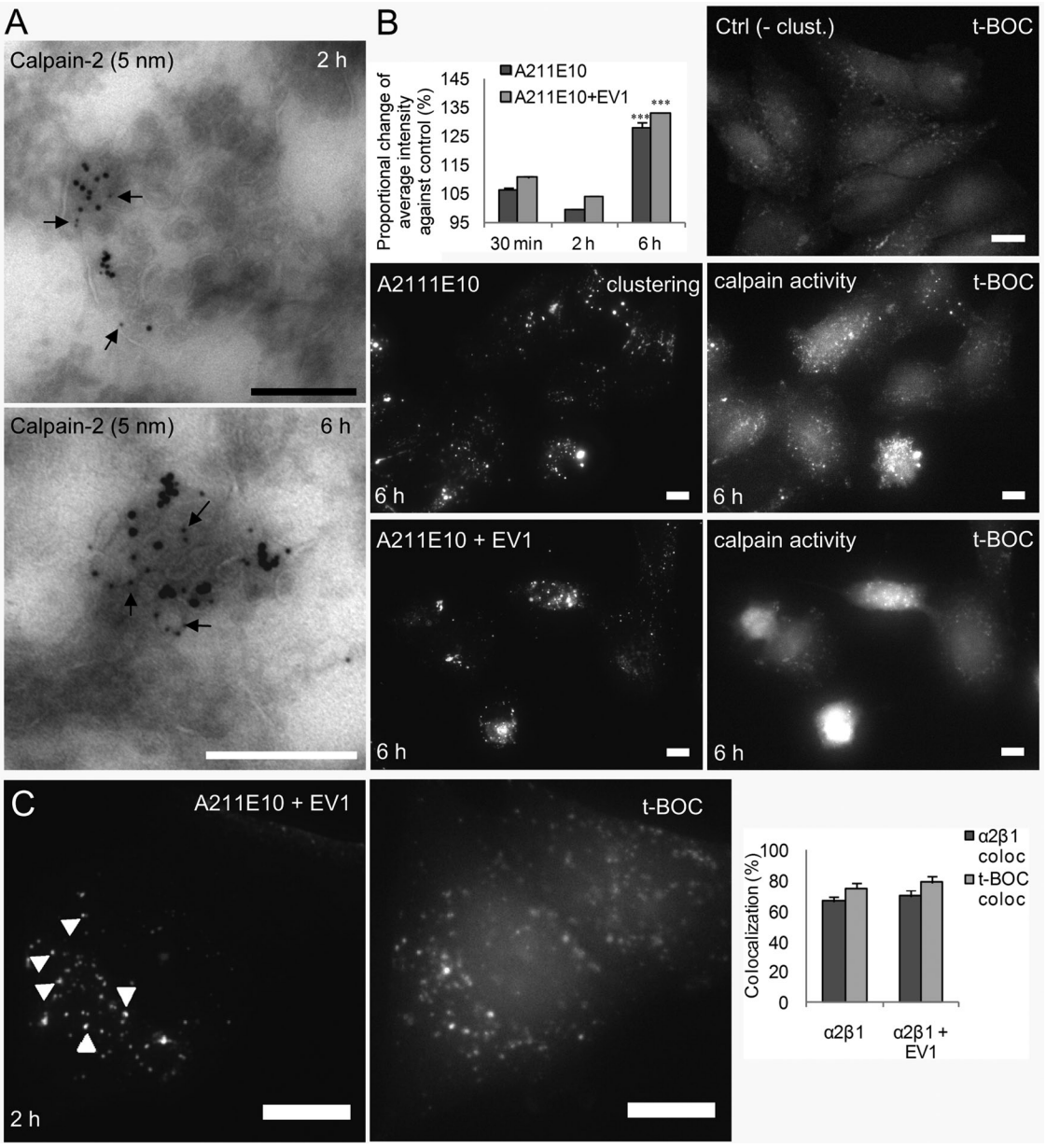

FIGURE 9: Calpains are present and active in α2-MVBs. (A) Calpain-2 antibody labeling of thin, frozen sections. The amount of small gold particles representing calpain label from 30 α2-MVB structures were counted and compared with labeling with control IgG. Calculated p values were $p < 0.005$ for 2 h and $p < 0.0002$ for 6-h samples. (B) t-BOC intensity was measured from the wide-field images after 30 min, 2 h, and 6 h of α2 integrin clustering and internalization with or without EV1. The change of intensities was compared with the basal calpain intensity in control cells (set to 100%). Intensity of t-BOC labeling was quantified from ~300 cells from three independent experiments (±SE). Example images after integrin clustering (A211E10) for 6 h with or without EV1 are shown. In addition, control t-BOC labeling from control unclustered cells is shown (Ctrl). Bars, 10 μm. (C) Wide-field images of t-BOC labeling in cells after α2 integrin clustering for 2 h ± EV1. Colocalization of t-BOC with α2 integrin (t-BOC coloc) and α2 integrin with t-BOC (α2β1 coloc) was measured from wide-field images from ~300 cells from three independent experiments. Some colocalized vesicles are highlighted by arrowheads. Bars, 10 μm.

Studies with calpain inhibitors revealed that indeed calpains are essential for degradation of clustered α2 integrin. In addition, active calpains were colocalized with α2-MVBs in the cytoplasm, and calpain-1 was coimmunoprecipitated with clustered integrin. Calpains are cytosolic proteases that need Ca^{2+} and a neutral environment to be active (Goll *et al.*, 2003; Suzuki and Sorimachi, 1998). The increase of calpain activity that was found after integrin clustering was in a similar range as found for calpain activation, for example, after myocardial injury induced by increased Ca^{2+} in the cytoplasm (Matsumura *et al.*, 2001). The maximal increase in calpain activity using t-BOC was 1.38-fold compared with the basal calpain activity in myocardial cells, and α2 integrin clustering here caused a 1.39-fold increase after 6 h. Similarly, in another study with t-BOC, calcium release from ER caused a 1.4-fold increase in calpain activity compared with basal activity (Rosser *et al.*, 1993).

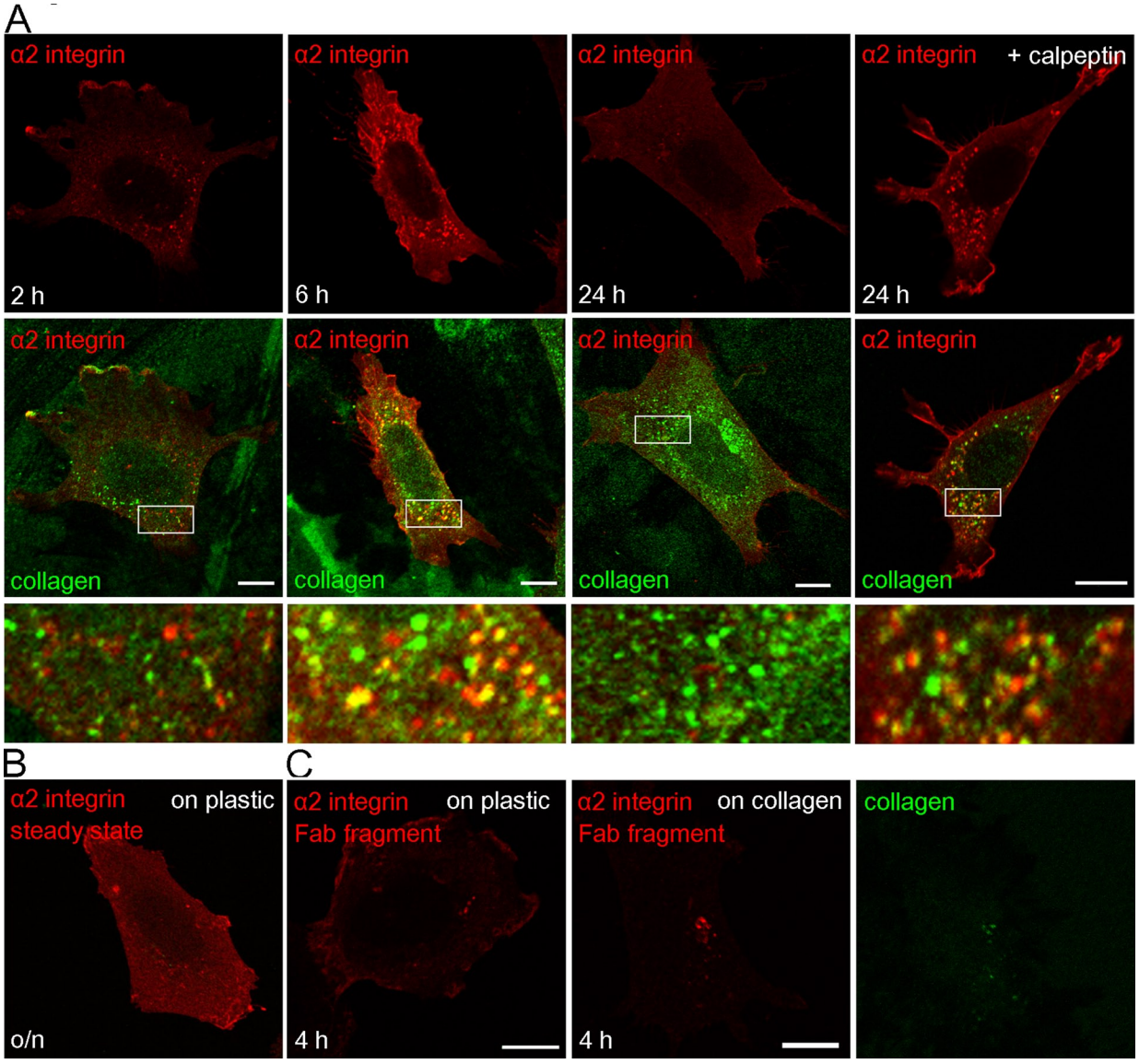

FIGURE 10: α2β1integrin distribution in cells plated on collagen. (A) Steady-state distribution of integrin (red) and collagen type I (green) after 2, 6, and 24 h with or without calpeptin. Merged images of integrin and collagen are below, with details shown in blow-up images. (B) Control integrin labeling of cells cultivated on plastic. Images in A and B were scanned with similar confocal intensity settings for easier comparison. (C) Surface labeling of α2β1 integrin by A211E10 antibody, followed by monovalent goat anti–mouse Fab549 DyLight (red) on cells cultivated on plastic (left) or on collagen coating (right) for 2 h. After surface labeling, cells were further incubated for 2 h, fixed, and labeled for collagen (green). Bars, 10 μm.

It is widely known that calpains regulate cell migration. Numerous calpain substrates are involved in cell migration and adhesion. These include, for example, talin, spectrin, and FAK (Franco and Huttenlocher, 2005). In addition, integrin β cytoplasmic tails, including β1 integrin, can be cleaved with calpain (Pfaff *et al.*, 1999). Calpains seem to have different kinds of roles in the regulation of adhesion sites, cell spreading, and formation of protrusions (Franco and Huttenlocher, 2005; Lebart and Benyamin, 2006). Calpain inhibition has been shown to reduce both β1 and β3 integrin–mediated cell migration by stabilizing cytoskeletal linkages and reducing detachment of adhesions at cell rear (Huttenlocher *et al.*, 1997; Palecek *et al.*, 1998). On the other hand, calpain can also induce the formation of early integrin clusters, which contain Rac-binding protein(s), calpain, and calpain-cleaved β3 integrin (Bialkowska *et al.*, 2000).

In this study we described an integrin down-regulation pathway that relies on calpains rather than lysosomal enzymes. Previously calpain was shown to contribute to down-regulation of β1 integrin in normal but not in cancer prostate cells in addition to lysosomal proteolysis (Moro *et al.*, 2004). Here we showed that calpains were efficiently precipitated together with clustered and unclustered α2 and β1 integrins and were active in the internalized structures. Calpains are known to be activated after ligand binding to integrin close to the plasma membrane (Fox *et al.*, 1993; Carragher *et al.*, 1999). The coprecipitated calpain after 2 h was predominantly the smaller autolysed 78- or 76-kDa form of calpain-1, suggesting that during clustering and internalization calpains were indeed activated (Hathaway *et al.*, 1982; Cong *et al.*, 1989; Zimmerman and Schlaepfer, 1991; Schoenwaelder *et al.*, 1997). Calpain autolysis has

been associated with activation of calpains (Inomata *et al.*, 1986; Cong *et al.*, 1989; Baki *et al.*, 1996; Suzuki and Sorimachi, 1998). However, autolysis is not essential for calpain catalytic activation since intact calpains can also be active, but autolysis is thought to decrease the need of calcium for calpain activation (Imajoh *et al.*, 1986; Elce *et al.*, 1997; Suzuki and Sorimachi, 1998; Goll *et al.*, 2003). In addition, other factors—for example, phospholipid binding, regulation by cellular inhibitors, and the phosphorylation status of calpains—have been suggested to contribute to local activation of calpains (Franco and Huttenlocher, 2005). High calcium requirement for calpain activation may have been developed during evolution as a safety measure to inhibit unwanted proteolysis, and, for the same reason, it has been suggested that calpains would normally act with half-maximal efficiency.

What is the mechanism of calpain-mediated degradation of the integrins? Calpains are not normally accessible to the N-terminal luminal domain of α2β1 integrin, which was evidently degraded after clustering and internalization. Therefore, during the internalization process, in the forming α2-MVBs, calpains need to gain better access to the integrin substrate. Calpeptin did not prevent the formation of α2-MVBs, suggesting that the inhibition of degradation does not occur through a block in structural morphogenesis. The observation that the integrin structures were clearly less acidic than late endosomes/lysosomes may be one crucial factor for efficient calpain action. This is also demonstrated by the fact that EV1-triggered structures showed more-enhanced integrin degradation and remained in slightly higher pH than structures triggered by antibody-induced clustering. Calpains are known to associate with α2β1 integrin C-termini on the plasma membrane. Our EM immunolabeling results suggested that during the biogenesis of α2-MVBs calpains are associated with endosomal limiting membrane, and they may be partially targeted to the forming intraluminal vesicles, as they remain bound to α2 integrin. Our studies indicated that also the luminal domains of integrins, not only the beta tail (Pfaff *et al.*, 1999), undergo degradation by calpains. Viruses are known to cause endosomal membrane ruptures, including another picornavirus major group rhinovirus, HRV14 (Schober *et al.*, 1998), and human adenovirus after binding to its integrin receptor αVβ5 (Wickham *et al.*, 1994; Greber *et al.*, 1996). Our preliminary results suggest that increased permeability of α2-MVBs and ruptures of intraluminal vesicles are detected during EV1 entry by a novel confocal microscopy assay and cryo–electron tomography, respectively (Soonsawad, Upla, Weerachatyanukul, Rintanen, Poon, Cheng, Espinoza, McNerney, Huser, Hwang, Milla, Tripathi, Pisitchaiyakul, Furukawa, Kawasaki, Vahlne, Marjomäki, Cheng, unpublished results). Calpains may thus enter the endosomal lumen through the formed breakages. In the endosomal lumen the Ca^{2+} concentration is supposedly higher than in the cytoplasm, thus leading to higher calpain activation. This is in line with our fluorescent t-BOC activity labelings, which suggested higher activity in large clusters, especially after 6 h of internalization. One can speculate that integrin clustering on the plasma membrane may lead to recruitment of crucial factors or to the release of inhibitory factors and higher activation of calpains in the α2-MVBs. We showed recently that expression of the dominant-negative Vps4, which decreases the formation of ILVs in the MVBs, leads to reduced turnover of integrin in the α2-MVBs, suggesting further that ILVs may be important in the calpain-dependent turnover of integrins (Karjalainen *et al.*, 2011). To have full understanding of this process of calpain activation in α2-MVBs more biochemical and structural studies are needed.

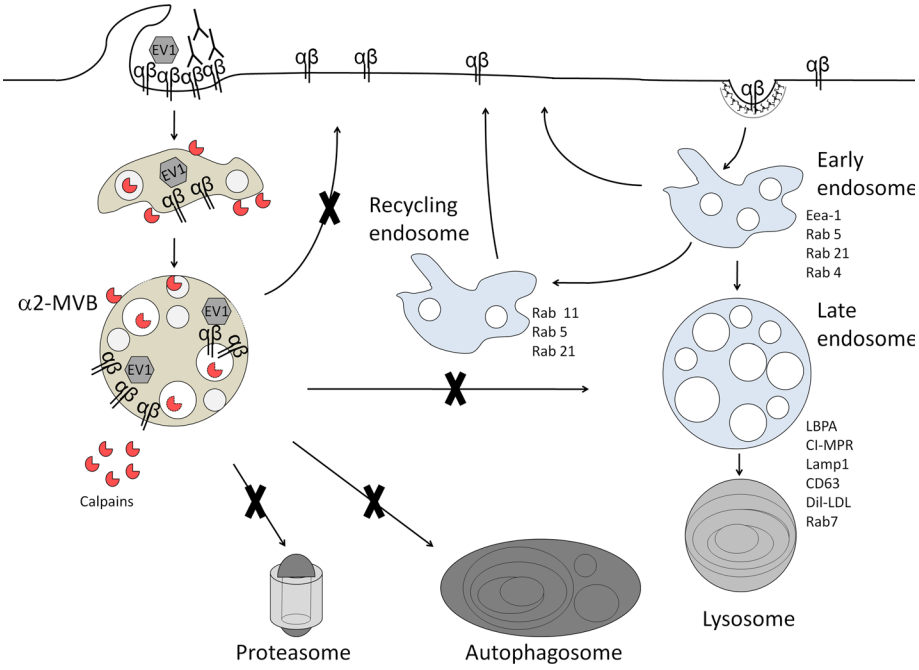

FIGURE 11: Integrin clustering induced a down-regulation pathway. After clustering of α2β1 integrin on the plasma membrane with EV1 or antibodies, integrin is internalized to the perinuclear region and accumulates in α2-MVBs. Integrin is not recycled back to the plasma membrane, in contrast to the slow recycling of the unclustered α2 integrin. The perinuclear α2-MVBs are degradative structures and distinct from lysosomes, autophagosomes, and proteasomes. Instead, degradation of integrin in α2-MVBs is promoted by neutral proteases—calpains that are present and activated in these structures.

It is surprising that exposure of cells on collagen—the physiological ligand of α2β1 integrin—induced collagen and integrin uptake to cells, resembling the effects of antibody clustering or EV1 infection. The integrin was targeted to cytoplasmic vesicles, leading to calpain-sensitive turnover during 24 h. This suggests that EV1 may have evolved to use a similar pathway that is elicited during uptake of soluble collagen. Previously the urokinase plasminogen activator receptor–associated protein (uPARAP)/Endo180 was shown to be the crucial receptor for collagen uptake, whereas function-blocking antibodies against β1 integrins did not interfere with collagen uptake (Engelholm *et al.*, 2003). Despite the dispensable role of integrins in collagen uptake, integrin clustering upon collagen binding clearly can trigger integrin uptake and may be relevant for regulating integrin turnover. Further studies are needed to understand in detail the relationship between the cellular collagen uptake pathway and the clustering-induced integrin internalization pathway described here.

In conclusion (Figure 11), we suggest that after clustering of α2β1 integrin on the plasma membrane, integrin is internalized to the perinuclear region and accumulated in α2-MVBs, as we previously showed (Karjalainen *et al.*, 2008). Integrin is not recycled back to the plasma membrane, in contrast to the slow recycling of the

unclustered α2 integrin. The perinuclear α2-MVBs are degradative structures and distinct from lysosomes, autophagosomes, and proteasomes. Instead, degradation of α2 integrin in α2-MVBs is promoted by neutral proteases—calpains—which are accumulated and activated in these structures.

MATERIALS AND METHODS

Cells, viruses, antibodies, and reagents

Experiments were performed using a human osteosarcoma cell line overexpressing the α2 integrin subunit (SAOS-α2β1 cells, clone 45; Ivaska *et al*., 1999). EV1 (Farouk strain; American Type Culture Collection, Manassas, VA) was produced and purified as described previously (Marjomäki *et al*., 2002). The following polyclonal antibodies were used: rabbit antisera against purified EV1 (Marjomäki *et al*., 2002), calpain-2 (Sigma-Aldrich, St. Louis, MO), α2 integrin (a gift from Jyrki Heino, University of Turku, Turku, Finland), α2 integrin (AB1936; Millipore, Billerica, MA), CI-MPR (Marjomäki *et al*., 1990), Rab7 (a gift from Jean Gruenberg, University of Geneva, Geneva, Switzerland), collagen type I (Cedarlane Laboratories, Burlington, NC), Alexa 488 (Invitrogen, Carlsbad, CA), mouse IgG (Sigma-Aldrich), and rat IgG (Jackson ImmunoResearch Laboratories, West Grove, PA). In addition, goat anti–rabbit or anti–mouse IgG conjugated with Alexa 488, Alexa 555, Alexa 594, fluorescein (Invitrogen), or HRP (Bio-Rad Hercules, CA) and goat anti–mouse or anti–rabbit Fab fragment DyLight 549 (Jackson ImmunoResearch) were used. Monoclonal antibodies against α2 integrin (A211E10 [from Fedor Berditchevski, Institute of Cancer Studies, Birmingham, United Kingdom] and MCA2025 [AbD Serotec, Raleigh, NC]), β1 integrin (12G10 [Abcam, Cambridge, MA] and Mab13 [BD Biosciences PharMingen, San Diego, CA]), CD63 (Zymed, San Francisco, CA), Lamp-1 (Santa Cruz Biotechnology, Santa Cruz, CA), EGFR (Thermo Scientific, Waltham, MA), EEA1, and calpain-1 (Sigma-Aldrich) were used.

Aprotinin, elastatinal, leupeptin, soybean trypsin inhibitor, antipain, EGF, and octyl-β-glucopyranoside were all purchased from Sigma-Aldrich. Calpeptin, lactacystin, bafilomycin, nigericin, and calpain-1 and -2 inhibitors were from Calbiochem (La Jolla, CA). FuGENE 6 reagent was purchased from Roche (Indianapolis, IN), t-BOC substrate and streptavidin–Alexa 488 from Invitrogen, and bortezomib from LC Laboratories (Woburn, MA). LC3-GFP was a gift from Eeva-Liisa Eskelinen (University of Helsinki, Helsinki, Finland). Supersignal chemiluminescent substrate was purchased from Pierce Thermo Fisher Scientific (Rockford, IL), Vitrogen 100 from Angiotech BioMaterials (Palo Alto, CA), PA-Sepharose from GE Healthcare (Piscataway, NJ), and Easytag [^{35}S]methionine and cysteine labeling mix and En3hance solution from PerkinElmer (Waltham, MA). Dil-LDL was kindly provided by Seppo Ylä-Herttuala (University of Eastern Finland, Kuopio, Finland).

Viral infection and integrin clustering experiments

EV1 was used at multiplicity of infection of 100 in all experiments. EV1 was first bound to cells for 1 h on ice in DMEM containing 1% serum; cells were washed extensively and then put to +37°C in DMEM containing 10% serum to allow internalization. For infectivity testing, infection was allowed to proceed for 6 h. To test the effect of starvation on EV1 infectivity, cells were grown without serum overnight, and virus binding and following incubation were done in serum-free DMEM. In colocalization assays, virus was prelabeled with sequential treatments with anti-EV1 antibody and goat anti-rabbit Alexa antibody on ice before internalization. Prelabeling of EV1 has been verified not to affect infectivity. In the α2β1 integrin antibody clustering protocol, monoclonal antibody A211E10 or MCA2025 against α2 integrin was bound to cells in 1% DMEM for 45 min on ice. Cells were washed extensively and incubated with a clustering secondary antibody for 45 min. In nonclustering controls a monovalent Fab fragment of IgG was used instead. After washing, cells were incubated in DMEM containing 10% serum at +37°C to allow internalization. To measure the degradation of α2 integrin, clustering was done with MCA2025 and goat anti–mouse Alexa 555 antibodies. After fixation and permeabilization, α2 integrin was labeled with biotinylated A211E10 and streptavidin–Alexa 488.

Drug treatments

Cells were preincubated for 30 min with 10 μM lactacystin or 0.7 μM bortezomib before EV1 attachment or antibody clustering. Drugs were also present in the incubation medium. Bafilomycin (50 nM) was either added 15 min, 30 min, 1 h, or 2 h p.i. (infectivity testing) or 2 h p.i. (pH measurements) to the cells.

Six protease inhibitors were used: antipain (500 μM), aprotinin (1 μM), elastatinal (250 μM), leupeptin (108 μM), soybean trypsin inhibitor (75 μM), and calpeptin (50 μm). DMSO was used as control. Subconfluent SAOS-α2β1 cells were preincubated in 10% DMEM with drugs for 1 h (except for leupeptin overnight) before clustering, and inhibitor was also present in the incubation medium. α2 integrin was clustered as described. After each time point cells were lysed on ice with lysis buffer (150 mM NaCl, 1 mM $CaCl_2$, 1 mM $MgCl_2$, 25 mM Tris-HCl, pH 7.4) containing 100 mM octyl-β-glucopyranoside. From each sample the amount of total proteins was measured with Bradford assay. The amount of HRP conjugated to secondary antibody (Bio-Rad) was detected from color reaction, which was induced with reaction solution (0.0003% H_2O_2, 0.1% Triton X-100, 10 mg *o*-diniazidine, 0.05 M $NaPO_4$, pH 5.0). Absorbance of samples was measured at 405 nm, and the results were compared with HRP standards. Background peroxidase activity was removed from the results.

t-BOC assay

t-BOC substrate was added at 50 μM concentration on clustered cells 20 min before fixation and embedding in Mowiol. Cells were imaged with a Cell Observer wide-field microscope (Zeiss, Jena, Germany) using a 365-nm light-emitting diode for excitation of t-BOC and 590 nm for α2 integrin labeled with Alexa 594.

Collagen coating assay

Coverslips were coated with 5 μg/ml collagen (Vitrogen 100) in phosphate-buffered saline (PBS) on ice and incubated overnight at +4°C. Cells were plated on coated coverslips in 0.5% bovine serum albumin (BSA)–DMEM and incubated at +37°C 2, 6, or 24 h before fixing with 4% paraformaldehyde (PFA). In Fab-fragment labeling experiments, after 2 h of incubation, cells were placed on ice, and integrin was labeled first with A211E10 antibody and then with goat anti-mouse Fab fragment DyLight 549. Then incubation was continued for 2 h at +37°C.

Metabolic labeling

Cells were pulsed for 24 h in serum-free DMEM with 50 μCi/ml of [^{35}S]methionine and cysteine labeling mix. After pulse, cells were chased for 0, 24, 48, 72, or 96 h in 10% fetal calf serum (FCS)–DMEM with 0.16 mg/ml nonradioactive methionine. Cells were scraped, and pellet was dissolved in IP buffer (150 mM NaCl, 1 mM $CaCl_2$, 1 mM $MgCl_2$, 25 mM Tris-HCl, pH 7.4) containing 0.1 M octyl-β-D-glucopyranoside for 30 min on ice. α2 integrin antiserum was added to cleared supernatant and incubated overnight at +4°C and then precipitated with PA–Sepharose. When the precipitates were treated with calpain enzymes, calpain-1 (10 μg) or calpain-2 (5 μg) was

added on the precipitate samples for 5 and 60 min at +37°C. When used, calpain inhibitor calpeptin was added before calpain enzymes. Samples were separated by SDS–PAGE, and radioactive gels were treated with enhancer solution, dried, and exposed against X-ray film at −80°C. Band size and intensities from the film were analyzed with Adobe Photoshop (San Jose, CA).

Surface biotinylation, immunoprecipitation, and immunoblotting

Cells growing in 10% fetal bovine serum containing medium were placed on ice, and cell surface proteins were labeled with 0.5 mg/ml of EZ-Link sulfo-NHS-LC-biotin (Thermo Scientific) in Hank's balanced salt solution (Sigma-Aldrich) for 30 min at +4°C. Unbound biotin was washed away, and α2 integrins were clustered with A211E10 and rabbit anti–mouse antibodies as described. The negative control sample was incubated only with the secondary antibody. The biotinylated integrins were allowed to internalize at +37°C, after which cells were washed and lysed by scraping in lysis buffer (50 mM octyl-β-D-glucopyranoside, 1% NP-40, 0.5% BSA, 1 mM EDTA, with phosphatase and protease inhibitor cocktails [Roche]), followed by 20 min of incubation at +4°C. Cell extracts were cleared by centrifugation (16,000 × *g*, 10 min, +4°C), and the clustered integrins were immunoprecipitated with protein G–Sepharose beads (GE Healthcare) for 1 h at +4°C. The unclustered control samples were incubated with monoclonal α2 antibody (A211E10) for 1 h at +4°C before immunoprecipitation. Samples were separated on 7.5% SDS–PAGE gel, and the biotinylated integrins were detected from immunoblots with HRP-conjugated anti-biotin antibody (Cell Signaling Technology, Beverly, MA).

For total α2 integrin immunoprecipitation, polyclonal rabbit α2 integrin antibody (ab1936) was used. For β1 integrin immunoprecipitation rat β1 integrin antibody (Mab13) or mouse β1 integrin antibody (12G10) was used. Rabbit anti-rat or rabbit anti–mouse antibodies were bound to PA–Sepharose to immunoprecipitate Mab13 or 12G10, respectively. Samples were loaded and separated in 7.5% SDS–PAGE gel and electroblotted onto polyvinylidene fluoride membrane (Millipore). The blot was blocked for 1 h at room temperature with 5% BSA in 0.1% Tween-Tris buffered saline (TBS). Primary and secondary antibodies in 5% BSA and in 0.1% Tween-TBS were incubated for 1 h sequentially. The bands were detected by chemiluminescence with the ChemiDoc XRS gel documentation system (Bio-Rad).

Recycling assays

In the bleaching experiment, SAOS-α2β1 cells were cultivated on Lab-Tek eight-well plates (Nalge Nunc International, Rochester, NY). α2β1 integrin was clustered on ice as described. The plates were transferred to a Zeiss confocal setup and kept at +37°C. After integrin internalization for 2.5 h, edges of the cell were bleached completely with high-intensity laser excitation (40 iterations with argon laser were used). *z*-Sections through the cells were taken before and after bleaching and subsequently with 1-h intervals until 6.5 h.

In the recycling assay, using the quenching anti-Alexa antibody, EV1 was first bound on cells on ice, after which integrin was clustered with anti–α2 integrin antibody (MCA2025) and goat anti–mouse Alexa 488. After 1 h of internalization, all cells except nontreated samples were treated for 30 min on ice with 0.024 mg/ml anti–Alexa 488 antibody in 1% DMEM to quench fluorescence of the surface remaining Alexa 488 signal. Thereafter, cells were quenched after 1 h intervals with anti–Alexa 488 antibody on ice repetitively for 4 h. Control cells were treated with 1% DMEM. Samples after each quenching period were fixed and imaged on confocal microscopy. Intensity of fluorescence was analyzed from the confocal *z*-stacks with BioImageXD (a free, open source software package; Kankaanpää *et al.*, www.bioimagexd.net) segmentation tools.

Recycling was also evaluated using electron microscopy. SAOS-α2β1 cells were first treated with anti–α2 integrin antibody (A211E10), then with rabbit anti–mouse IgG (Sigma-Aldrich), and finally with 10 nm of PA-gold prepared according to Slot and Geuze (2007), all for 45 min on ice, followed by extensive washes. The cells were then transferred to 37°C and incubated for 2 or 24 h in 10% DMEM. The cells were fixed in 2.5% glutaraldehyde in 0.1 M phosphate buffer (pH 7.4) for 1 h, postfixed with 1% osmium tetroxide for 1 h in the same buffer, dehydrated in ethanol, stained with uranyl acetate, and embedded with LX-112.

Intraendosomal pH measurement

Intraendosomal pH measurements were conducted as previously described (Karjalainen *et al.*, 2011). Briefly, EV1 was first bound to SAOS-α2β1 cells on ice, followed by incubation with anti-EV1 antibody. Then equal amounts of goat anti–rabbit fluorescein and goat anti–rabbit Alexa 555 were bound to cells on ice and the cells moved to 37°C for 4–6 h. In antibody clustering, anti-integrin (A211E10) antibody and goat anti–mouse fluorescein and Alexa 555 were used. Bafilomycin (50 nM) was added on cells after 2 h. Cells were kept at +37°C in the Olympus FluoView 1000 confocal setup under CO_2-independent medium (Life Technologies, Carlsbad, CA) containing 10% serum. Confocal sections were taken at 4 and 6 h in the absence or presence of bafilomycin. For the pH titration curve, cell membranes were permeabilized with 20 µM nigericin in pH standard buffer solutions (150 mM KCl, 5 mM glucose, and 15 mM Tris, pH 7.0) or 15 mM 2-(*N*-morpholino)ethanesulfonic acid, pH 5.5, 6.0, and 6.5). Altogether 30 cells in each case from two independent tests were scanned, and the ratio of fluorescein/Alexa 555 was determined for each section. When pH of EGFR was measured, EGFR antibody against extracellular domain and equal amounts of goat anti–mouse fluorescein and Alexa 555 were bound sequentially on ice in serum-free conditions. EGF, 100 ng/ml, was used to internalize receptor at +37°C in serum-free, CO_2-independent medium. Cells were imaged with the confocal setup of the Zeiss LSM510.

Electron microscopy

For visualizing the internalized α2β1 integrin, cells were incubated with anti–α2 integrin antibody (A211E10) and subsequently with rabbit anti–mouse IgG and protein A gold and processed for EM as described previously (Upla *et al.*, 2004). Briefly, cells were fixed in 4% PFA containing 0.1% glutaraldehyde in 50 mM Tris buffer, pH 7.6, at room temperature for 1 h or at +4°C overnight. Cells were then dehydrated, stained with 2% uranylacetate, and embedded in LX-112 Epon. For cryoimmuno–EM, cells were treated as described recently (Karjalainen *et al.*, 2011). Briefly, clustered cells were fixed with 4% PFA-PBS for 10 min and scraped, with fixation continued up to 30 min, and pelleted by centrifugation. Cells were embedded in 12% gelatin-PBS and saturated overnight in 2.3 M sucrose. After cryosectioning, sucrose/methyl cellulose film was dissolved with extensive PBS washes, and free aldehyde groups were blocked with 0.1% glycine/PBS for 30 min. Sections were then blocked with 10% FCS/PBS for 20 min and washed twice with PBS. Sections were labeled for 30 min with primary antibodies rabbit calpain-2 or control IgG in 5% FCS/PBS and washed extensively with PBS. PA-gold (5 nm) was allowed to react for 20 min in 5% FCS/PBS, after which sections were washed with PBS and water and finally coated with methyl cellulose/uranyl acetate.

Immunofluorescence and confocal microscopy

SAOS-α2β1 cells were fixed with 4% PFA for 20–30 min, permeabilized with 0.2% Triton X-100 in PBS for 5 min, and treated with antibodies diluted in PBS containing 3% bovine serum albumin. For Rab7 labeling, cells were permeabilized with 0.05% saponin. Goat secondary antibodies (conjugated to Alexa dye 488, 555, or 594) against rabbit and mouse antibodies (Invitrogen) were used. The cells were mounted in Mowiol–1,4-diazabicyclo[2.2.2]octane and examined with an Axiovert 100 M SP epifluorescence microscope (Carl Zeiss) equipped with a confocal setup (Zeiss LSM510) or with an Olympus microscope IX81 with a FluoView-1000 confocal setup.

Data analysis of the microscopic data

Quantification of fluorescence intensity and colocalization was determined with BioImageXD. Levels for the laser power, detector amplification, and optical sections were optimized for each channel in the confocal microscope before starting the quantification. The colocalization thresholds were set manually to eliminate background fluorescence. Statistical significance of observed colocalization was calculated by Costes' algorithm (Costes *et al.*, 2004) embedded in software, and only colocalization with zero coincidence probability was taken into account (i.e., $p = 1.000$).

Fluorescence intensity of cells from confocal images was evaluated by intensity threshold segmentation. The intensity threshold was selected experimentally so that the background fluorescence was eliminated. Objects were defined from the background and connected objects separated with segmentation tools. Average intensity of the object was normalized to average area of the object or number of vesicles to produce sum of intensities.

t-BOC intensity was defined by first smoothing images with a Gaussian kernel. After that, fixed experimentally defined intensity threshold was used for all images, and all connected regions with fewer than three pixels were removed to eliminate photon shot noise. Regions for cell area calculation were defined by first smoothing images with a Gaussian kernel and thresholding using an automatic Otsu method.

To analyze recycling and degradation of α2β1 integrin, three-dimensional confocal images of single cells or two-dimensional images of multiple cells were first smoothed using a Gaussian kernel. The objects were then defined by sequential procedures using dynamic threshold, Euclidean distance mapping, and morphological watershed segmentation. From the resulting regions, total fluorescence was normalized by the cell number.

Statistical testing

Statistical pairwise comparison of samples was done with the *t* test. For percentages or ratio figures, the *t* test was applied after arcsine square root transformation of the original variable to convert the binomial distribution of the data to follow normal distribution.

ACKNOWLEDGMENTS

We thank Mari Koistinen and Arja Mansikkaviita for technical assistance. The Biocenter Oulu electron microscopy core facility is acknowledged for cutting thin, frozen sections. This work was supported by grants from the Academy of Finland, a European Research Council Starting Grant, the Finnish Cancer Organisations, the Sigrid Juselius Foundation, the Albin Johansson Foundation, and the National Graduate School in Nanoscience, University of Jyväskylä, Jyväskylä, Finland.

REFERENCES

Baki A, Tompa P, Alexa A, Molnar O, Friedrich P (1996). Autolysis parallels activation of mu-calpain. Biochem J 318, 897–901.

Bialkowska K, Kulkarni S, Du X, Goll DE, Saido TC, Fox JE (2000). Evidence that beta3 integrin-induced Rac activation involves the calpain-dependent formation of integrin clusters that are distinct from the focal complexes and focal adhesions that form as Rac and RhoA become active. J Cell Biol 151, 685–696.

Burke P, Schooler K, Wiley HS (2001). Regulation of epidermal growth factor receptor signaling by endocytosis and intracellular trafficking. Mol Biol Cell 12, 1897–1910.

Bruns AF, Herbert SP, Odell AF, Jopling HM, Hooper NM, Zachary IC, Walker JH, Ponnambalam S (2010). Ligand-stimulated VEGFR2 signaling is regulated by co-ordinated trafficking and proteolysis. Traffic 11, 161–174.

Carragher NO, Levkau B, Ross R, Raines EW (1999). Degraded collagen fragments promote rapid disassembly of smooth muscle focal adhesions that correlates with cleavage of pp125(FAK), paxillin, and talin. J Cell Biol 147, 619–630.

Caswell PT, Vadrevu S, Norman JC (2009). Integrins: masters and slaves of endocytic transport. Nat Rev Mol Cell Biol 10, 843–853.

Ciechanover A (2005). Proteolysis: from the lysosome to ubiquitin and the proteasome. Nat Rev Mol Cell Biol 6, 79–87.

Cong J, Goll DE, Peterson AM, Kapprell HP (1989). The role of autolysis in activity of the Ca2+-dependent proteinases (mu-calpain and m-calpain). J Biol Chem 264, 10096–10103.

Costes SV, Daelemans D, Cho EH, Dobbin Z, Pavlakis G, Lockett S (2004). Automatic and quantitative measurement of protein-protein colocalization in live cells. Biophys J 86, 3993–4003.

Demarchi F, Bertoli C, Copetti T, Tanida I, Brancolini C, Eskelinen EL, Schneider C (2006). Calpain is required for macroautophagy in mammalian cells. J Cell Biol 175, 595–605.

Elce JS, Hegadorn C, Arthur JS (1997). Autolysis, Ca2+ requirement, and heterodimer stability in m-calpain. J Biol Chem 272, 11268–11275.

Engelholm LH *et al.* (2003). uPARAP/Endo180 is essential for cellular uptake of collagen and promotes fibroblast collagen adhesion. J Cell Biol 160, 1009–1015.

Falguieres T, Luyet PP, Gruenberg J (2009). Molecular assemblies and membrane domains in multivesicular endosome dynamics. Exp Cell Res 315, 1567–1573.

Fox JE, Taylor RG, Taffarel M, Boyles JK, Goll DE (1993). Evidence that activation of platelet calpain is induced as a consequence of binding of adhesive ligand to the integrin, glycoprotein IIb-IIIa. J Cell Biol 120, 1501–1507.

Franco SJ, Huttenlocher A (2005). Regulating cell migration: calpains make the cut. J Cell Sci 118, 3829–3838.

Fuchs R, Blaas D (2010). Uncoating of human rhinoviruses. Rev Med Virol 20, 281–297.

Futter CE, Pearse A, Hewlett LJ, Hopkins CR (1996). Multivesicular endosomes containing internalized EGF-EGF receptor complexes mature and then fuse directly with lysosomes. J Cell Biol 132, 1011–1023.

Goll DE, Thompson VF, Li H, Wei W, Cong J (2003). The calpain system. Physiol Rev 83, 731–801.

Greber UF, Webster P, Weber J, Helenius A (1996). The role of the adenovirus protease on virus entry into cells. EMBO J 15, 1766–1777.

Hanna RA, Campbell RL, Davies PL (2008). Calcium-bound structure of calpain and its mechanism of inhibition by calpastatin. Nature 456, 409–412.

Hathaway DR, Werth DK, Haeberle JR (1982). Limited autolysis reduces the Ca2+ requirement of a smooth muscle Ca2+-activated protease. J Biol Chem 257, 9072–9077.

Huttenlocher A, Palecek SP, Lu Q, Zhang W, Mellgren RL, Lauffenburger DA, Ginsberg MH, Horwitz AF (1997). Regulation of cell migration by the calcium-dependent protease calpain. J Biol Chem 272, 32719–32722.

Imajoh S, Kawasaki H, Suzuki K (1986). Limited autolysis of calcium-activated neutral protease (CANP): reduction of the Ca2+-requirement is due to the NH2-terminal processing of the large subunit. J Biochem 100, 633–642.

Inomata M, Imahori K, Kawashima S (1986). Autolytic activation of calcium-activated neutral protease. Biochem Biophys Res Commun 138, 638–643.

Ivaska J, Reunanen H, Westermarck J, Koivisto L, Kähäri VM, Heino J (1999). Integrin alpha2beta1 mediates isoform-specific activation of p38 and upregulation of collagen gene transcription by a mechanism involving the alpha2 cytoplasmic tail. J Cell Biol 147, 401–416.

Ivaska J, Vuoriluoto K, Huovinen T, Izawa I, Inagaki M, Parker PJ (2005). PKCepsilon-mediated phosphorylation of vimentin controls integrin recycling and motility. EMBO J 24, 3834–3845.
Jokinen J *et al.* (2010). Molecular mechanism of alpha2beta1 integrin interaction with human echovirus 1. EMBO J 29, 196–208.
Jones MC, Caswell PT, Norman JC (2006). Endocytic recycling pathways: emerging regulators of cell migration. Curr Opin Cell Biol 18, 549–557.
Kankaanpää P, Paavolainen L, Marjomäki V, Heino J, White DJ. BioImageXD—free open source software for analysis and visualization of multidimensional biomedical images. Available at: www.bioimagexd.net (accessed 5 November 2011).
Karjalainen M, Kakkonen E, Upla P, Paloranta H, Kankaanpää P, Liberali P, Renkema GH, Hyypiä T, Heino J, Marjomäki V (2008). A Raft-derived, Pak1-regulated entry participates in alpha2beta1 integrin-dependent sorting to caveosomes. Mol Biol Cell 19, 2857–2869.
Karjalainen M, Rintanen N, Lehkonen M, Kallio K, Maki A, Hellstrom K, Siljamaki V, Upla P, Marjomaki V (2011). Echovirus 1 infection depends on biogenesis of novel multivesicular bodies. Cell Microbiol 13, 1975–1995.
Khor R, McElroy LJ, Whittaker GR (2003). The ubiquitin-vacuolar protein sorting system is selectively required during entry of influenza virus into host cells. Traffic 4, 857–868.
Le Blanc I *et al.* (2005). Endosome-to-cytosol transport of viral nucleocapsids. Nat Cell Biol 7, 653–664.
Lebart MC, Benyamin Y (2006). Calpain involvement in the remodeling of cytoskeletal anchorage complexes. FEBS J 273, 3415–3426.
Liberali P *et al.* (2008). The closure of Pak1-dependent macropinosomes requires the phosphorylation of CtBP1/BARS. EMBO J 27, 970–981.
Lobert VH, Brech A, Pedersen NM, Wesche J, Oppelt A, Malerod L, Stenmark H (2010). Ubiquitination of alpha 5 beta 1 integrin controls fibroblast migration through lysosomal degradation of fibronectin-integrin complexes. Dev Cell 19, 148–159.
Marjomäki VS, Huovila AP, Surkka MA, Jokinen I, Salminen A (1990). Lysosomal trafficking in rat cardiac myocytes. J Histochem Cytochem 38, 1155–1164.
Marjomäki V, Pietiäinen V, Matilainen H, Upla P, Ivaska J, Nissinen L, Reunanen H, Huttunen P, Hyypiä T, Heino J (2002). Internalization of echovirus 1 in caveolae. J Virol 76, 1856–1865.
Matsumura Y, Saeki E, Otsu K, Morita T, Takeda H, Kuzuya T, Hori M, Kusuoka H (2001). Intracellular calcium level required for calpain activation in a single myocardial cell. J Mol Cell Cardiol 33, 1133–1142.
Mercer J, Schelhaas M, Helenius A (2010). Virus entry by endocytosis. Annu Rev Biochem 79, 803–833.
Moro L, Perlino E, Marra E, Languino LR, Greco M (2004). Regulation of beta1C and beta1A integrin expression in prostate carcinoma cells. J Biol Chem 279, 1692–1702.
Ng T, Shima D, Squire A, Bastiaens PI, Gschmeissner S, Humphries MJ, Parker PJ (1999). PKCalpha regulates beta1 integrin-dependent cell motility through association and control of integrin traffic. EMBO J 18, 3909–3923.
Palecek SP, Huttenlocher A, Horwitz AF, Lauffenburger DA (1998). Physical and biochemical regulation of integrin release during rear detachment of migrating cells. J Cell Sci 111, 929–940.
Pellinen T, Arjonen A, Vuoriluoto K, Kallio K, Fransen JA, Ivaska J (2006). Small GTPase Rab21 regulates cell adhesion and controls endosomal traffic of beta1-integrins. J Cell Biol 173, 767–780.
Pellinen T, Ivaska J (2006). Integrin traffic. J Cell Sci 119, 3723–3731.
Pfaff M, Du X, Ginsberg MH (1999). Calpain cleavage of integrin beta cytoplasmic domains. FEBS Lett 460, 17–22.
Pietiäinen V, Marjomäki V, Upla P, Pelkmans L, Helenius A, Hyypiä T (2004). Echovirus 1 endocytosis into caveosomes requires lipid rafts, dynamin II, and signaling events. Mol Biol Cell 15, 4911–4925.
Pillay CS, Elliott E, Dennison C (2002). Endolysosomal proteolysis and its regulation. Biochem J 363, 417–429.
Powelka AM, Sun J, Li J, Gao M, Shaw LM, Sonnenberg A, Hsu VW (2004). Stimulation-dependent recycling of integrin beta1 regulated by ARF6 and Rab11. Traffic 5, 20–36.
Rosser BG, Powers SP, Gores GJ (1993). Calpain activity increases in hepatocytes following addition of ATPDemonstration by a novel fluorescent approach. J Biol Chem 268, 23593–23600.
Salazar G, Gonzalez A (2002). Novel mechanism for regulation of epidermal growth factor receptor endocytosis revealed by protein kinase A inhibition. Mol Biol Cell 13, 1677–1693.
Schober D, Kronenberger P, Prchla E, Blaas D, Fuchs R (1998). Major and minor receptor group human rhinoviruses penetrate from endosomes by different mechanisms. J Virol 72, 1354–1364.
Schoenwaelder SM, Kulkarni S, Salem HH, Imajoh-Ohmi S, Yamao-Harigaya W, Saido TC, Jackson SP (1997). Distinct substrate specificities and functional roles for the 78- and 76-kDa forms of mu-calpain in human platelets. J Biol Chem 272, 24876–24884.
Sigismund S, Argenzio E, Tosoni D, Cavallaro E, Polo S, Di Fiore PP (2008). Clathrin-mediated internalization is essential for sustained EGFR signaling but dispensable for degradation. Dev Cell 15, 209–219.
Slot JW, Geuze HJ (2007). Cryosectioning and immunolabeling. Nat Protoc 2, 2480–2491.
Suzuki K, Ohno S (1990). Calcium activated neutral protease–structure-function relationship and functional implications. Cell Struct Funct 15, 1–6.
Suzuki K, Sorimachi H (1998). A novel aspect of calpain activation. FEBS Lett 433, 1–4.
Tompa P, Buzder-Lantos P, Tantos A, Farkas A, Szilagyi A, Banoczi Z, Hudecz F, Friedrich P (2004). On the sequential determinants of calpain cleavage. J Biol Chem 279, 20775–20785.
Upla P, Marjomäki V, Kankaanpää P, Ivaska J, Hyypiä T, Van Der Goot FG, Heino J (2004). Clustering induces a lateral redistribution of alpha 2 beta 1 integrin from membrane rafts to caveolae and subsequent protein kinase C-dependent internalization. Mol Biol Cell 15, 625–636.
Upla P, Marjomäki V, Nissinen L, Nylund C, Waris M, Hyypiä T, Heino J (2008). Calpain 1 and 2 are required for RNA replication of echovirus 1. J Virol 82, 1581–1590.
van der Flier A, Sonnenberg A (2001). Function and interactions of integrins. Cell Tissue Res 305, 285–298.
van der Goot FG, Gruenberg J (2006). Intra-endosomal membrane traffic. Trends Cell Biol 16, 514–521.
van Kerkhof P, Lee J, McCormick L, Tetrault E, Lu W, Schoenfish M, Oorschot V, Strous GJ, Klumperman J, Bu G (2005). Sorting nexin 17 facilitates LRP recycling in the early endosome. EMBO J 24, 2851–2861.
Wickham TJ, Filardo EJ, Cheresh DA, Nemerow GR (1994). Integrin alpha v beta 5 selectively promotes adenovirus mediated cell membrane permeabilization. J Cell Biol 127, 257–264.
Wong J, Zhang J, Si X, Gao G, Mao I, McManus BM, Luo H (2008). Autophagosome supports coxsackievirus B3 replication in host cells. J Virol 82, 9143–9153.
Yoon SY, Ha YE, Choi JE, Ahn J, Lee H, Kweon HS, Lee JY, Kim DH (2008). Coxsackievirus B4 uses autophagy for replication after calpain activation in rat primary neurons. J Virol 82, 11976–11978.
Yuseff MI, Farfan P, Bu G, Marzolo MP (2007). A cytoplasmic PPPSP motif determines megalin's phosphorylation and regulates receptor's recycling and surface expression. Traffic 8, 1215–1230.
Zimmerman UJ, Schlaepfer WW (1991). Two-stage autolysis of the catalytic subunit initiates activation of calpain I. Biochim Biophys Acta 1078, 192–198.